RAMBOLL ENVIRON

FINAL REPORT

Improvements to CAMx Snow Cover Treatments and Carbon Bond Chemical Mechanism for Winter Ozone

UDAQ PO 480 52000000001

Prepared for:
Patrick Barickman
Utah Department of Environmental Quality
Division of Air Quality
195 North 1950 West
Salt Lake City, UT, 84116

Prepared by:
Chris Emery, Jaegun Jung, Bonyoung Koo, Greg Yarwood
Ramboll Environ
773 San Marin Drive, Suite 2115
Novato, California, 94998

August 2015

06-35838

CONTENTS

APPENDICES

TABLES

FIGURES

EXECUTIVE SUMMARY

Winter ozone formation events in areas such as the Uinta Basin occur under cold conditions that differ substantially from traditional summer ozone events. Snow cover influences wintertime ozone formation by several mechanisms: (1) increasing surface albedo and thus the total amount of ultraviolet (UV) irradiance for photolysis; (2) promoting formation of shallow, stable atmospheric layers near the ground; (3) inhibiting removal of emissions and secondary products by supressing surface deposition, and; (4) potentially introducing heterogeneous chemical reactions in the snowpack and forming products that can volatilize back into the air and sustain or increase ozone production. Photochemical mechanisms for ozone formation were first developed for summer ozone conditions and may not adequately describe ozone formation under cold conditions.

Ramboll Environ has developed and evaluated specific updates to the Comprehensive Air quality Model with extensions (CAMx) to improve the simulation of wintertime photochemistry. We improved the characterization of snow cover and its influence on atmospheric photolysis, dry deposition of gases and particles, and surface chemistry. We updated the Carbon Bond chemical mechanism (CB6r3) to account for the influence of temperature and pressure on the formation of organic nitrates from reactions of volatile organic compounds (VOC) and nitrogen oxides (NOx). These chemistry updates were transferred to model developers at the US Environmental Protection Agency (EPA), who incorporated CB6r3 into the Community Multi-scale Air Quality (CMAQ) model.

The CAMx updates were tested in simulations using model inputs provided by the Utah Division of Air Quality (UDAQ). The updates improve ozone simulations for the Uinta Basin by producing changes that are in line with expectations with respect to direction and magnitude. The updates to air chemistry in CB6r3 lower NOx at cold temperatures, which reduces ozone production slightly (<5 ppb) in our tests. The updates to the snow treatment increase surface albedo, thereby increasing photolysis, and reducing deposition rates for ozone and precursors. Collectively these snow modifications increase ozone moderately (5-10 ppb) in our tests. Surface chemistry on or within the snowpack may be a source of photochemically reactive compounds such as nitrous acid (HONO) that promote ozone production. Recent literature reviews conclude that snow chemistry mechanisms are complex, uncertain, and inconclusive, with more research needed. Tests of the snow surface chemistry model confirm functionality, but cannot determine whether or not snow chemistry is important in the Uinta basin because more research is needed to specify model parameters. The CAMx snow surface chemistry model can be used to test and evaluate results from future field experiments in the Uinta basin.

The model updates described here are insufficient by themselves to simulate ozone at measured levels throughout the Uinta Basin. The model exhibits strong sensitivity when NOx and VOC emission estimates are adjusted to better align with measurements recorded during the 2013 Uinta Basin Ozone Study (UBOS). But, even after NOx and VOC emission adjustments, the relative proportions of NOx oxidation products and certain individual VOC species remain incorrectly replicated, indicating that the simulated emission-chemistry cycle is not correct.

Several recommendations are provided for further improvements to the Uinta Basin emission inventory that would improve ozone model performance.

1.0 INTRODUCTION

Winter ozone formation events in areas such as the Uinta Basin occur under cold conditions that differ substantially from traditional summer ozone events. Snow cover influences wintertime ozone formation by several mechanisms: (1) increasing surface albedo and thus the total amount of ultraviolet (UV) irradiance for photolysis; (2) promoting formation of shallow, stable atmospheric layers near the ground; (3) inhibiting removal of emissions and secondary products by supressing surface deposition, and; (4) potentially introducing heterogeneous chemical reactions in the snowpack and forming products that can volatilize back into the air and sustain or increase ozone production. Photochemical mechanisms for ozone formation were first developed for summer ozone conditions and may not adequately describe ozone formation under cold conditions.

Winter ozone events in the Uinta Basin are being simulated by the Utah Division of Air Quality (UDAQ) using the Comprehensive Air quality Model with extensions (CAMx; ENVIRON, 2014) and the Community Multi-scale Air Quality (CMAQ) model (Byun and Schere, 2006). Both are state-of-the-science photochemical grid models (PGMs) that use Carbon Bond (CB) chemical mechanisms – version CB05-TU in CMAQ (Whitten et al., 2010) and version CB6r2 in CAMx (Hildebrandt Ruiz and Yarwood, 2013). Both models have under predicted observed ozone events in the Uinta Basin by factors of 2 or more, indicating fundamental errors in the representation of emissions and meteorology, and/or shortcomings in the models' chemical and physical treatments in simulating winter environments.

This report documents the development and evaluation of specific updates to CAMx to improve the simulation of wintertime photochemistry in areas such as the Uinta Basin. We improved the characterization of snow cover and its influence on atmospheric photolysis, dry deposition of gases and particles, and surface chemistry. We updated the Carbon Bond chemical mechanism (CB6r3) to account for the influence of temperature and pressure on the formation of organic nitrates from reactions of volatile organic compounds (VOC) and nitrogen oxides (NOx). These chemistry updates were transferred to model developers at the US Environmental Protection Agency (EPA), who incorporated CB6r3 into CMAQ.

The remainder of this section summarizes how snow cover was originally treated in CAMx and introduces some potentially important air chemistry issues pertinent to the Uinta Basin. Section 2 presents the approach to improve the CAMx snow cover treatment and the CB mechanism. Section 3 describes tests of the CAMx updates and analyses against measurement data. Section 4 presents our conclusions and recommendations. A full listing of the enhanced chemical mechanism developed in this study is provided in Appendix A.

1.1 CAMx Snow Cover

The starting point for this project is CAMx v6.1. CAMx ingests snow cover and other pertinent meteorological input fields from "off-line" meteorological simulations using such models as the Weather Research and Forecasting (WRF) model (Skamarock et al., 2008). Snow cover in v6.1

and all previous versions is characterized by a simple time-varying binary flag (0=no snow, 1=snow) set for each surface grid cell.

Photolysis rates are also externally developed using a radiative transfer model (TUV; NCAR, 2011), which builds a multi-dimensional lookup table for CAMx by photolytic reaction, solar angle, altitude, total atmospheric column ozone, and surface albedo. The surface albedo dimension of the photolysis lookup table contains five bins, two for the snow-free range (0.04 and 0.08) and three that represent snow cover (0.2, 0.5 and 0.8). For snow-covered grid cells, v6.1 sets the surface albedo to the middle snow value (0.5) to represent average conditions according to a previous literature review (Herman and Celarier, 1997). The other snow bins are not used in v6.1, but are included to support refinements that account for variable snow albedo.

CAMx offers two dry deposition options: Wesely (1989) or Zhang et al. (2003). In both cases, deposition is treated as a first-order flux (deposition velocity) that is a function of chemical species, meteorology, and surface parameters. Snow cover effects are implicitly included in Wesely's predetermined seasonal surface parameters and are thus not directly manipulated. The Zhang approach includes one set of baseline surface parameters that are weighted by monthly leaf area index (LAI) to account for seasonal variability, and then explicitly adjusted by fractional snow cover. The Zhang option in v6.1 assumes 80% snow cover when the snow flag is set to 1 in any grid cell.

A new surface chemistry model is introduced in CAMx v6.1. The model treats user-defined heterogeneous and photolysis reactions among selected compounds deposited on vegetative and bare ground surfaces, and allows volatile products to be re-emitted back to the atmosphere. Vegetated and bare ground fractions are internally set according to land cover type. The model was recently tested for an application in Houston, Texas (Lefer et al., 2014) to simulate the production and emission of nitrous acid (HONO) from surface reactions involving deposited NO_2 and nitric acid (HNO_3). The surface model implementation in v6.1 is tied to the Wesely deposition option and does not include specific treatments for snow covered surfaces.

1.2 Air Chemistry in Cold Environments

The inorganic chemical reactions (i.e., describing NOx, HOx, O_3, CO, HNO_3) included in CB and other well-vetted chemical mechanisms are based on data that have been peer reviewed for applicability to the global troposphere (Atkinson et al., 2004) and thus are suitable for modeling winter ozone. The state of knowledge for reactions involving simple organics (i.e., methane, ethane, formaldehyde, acetaldehyde) is comparable to that for inorganic reactions.

For larger organic molecules (i.e., propane and larger) the temperature dependencies of reaction rate constants are generally known for tropospheric conditions. However, any temperature dependencies of the products formed by organic reactions are poorly known for tropospheric conditions. Carter and Seinfeld (2012) considered how the Statewide Air Pollution Research Center (SAPRC) chemical mechanism should be modified for winter ozone and made a

special version of the mechanism that is better suited for such conditions (at the expense of suitability for summer conditions).

Winter ozone events have occurred to date where oil and gas exploration and production activities emit ozone precursors, and the most abundant organic compounds present in those environments are alkanes. Two temperature dependencies that affect the products formed from alkanes are:

1. Competition between alkoxy radical (RO) thermal decomposition (RO $\rightarrow$ products) and reaction with oxygen (RO + O2 $\rightarrow$ different products). Thermal decomposition is favored in warm temperatures. CB mechanisms (CB4, CB05, CB6) explicitly account for this temperature dependency.
2. Competition between formation of NO_2 and organic nitrates ($R\text{-}ONO_2$) when alkyl peroxy radicals (RO_2) react with NO. Organic nitrate formation is favored in cold temperatures. Carbon Bond mechanisms do not account for this effect but the temperature dependency has been studied (Arey et al., 2001) and so can be readily added.

Lee et al. (2014) considered how cold winter conditions in the Uinta Basin will affect organic nitrates and concluded (without conducting ozone modeling) that omitting the temperature dependence may cause 15% high bias in ozone formation. Photochemical grid modeling is needed to provide a more definitive evaluation of this question.

2.0 APPROACH

2.1 Updates to CAMx Snow Treatments

2.1.1 Snow Albedo

We have improved the treatment of surface albedo in CAMx by accessing additional snow variable fields routinely available from WRF. Specifically, albedo is now calculated according to snow depth (from snow water equivalent; SWE), snow age, and land cover type. The new albedo treatment completely replaces the original approach, which simply set surface albedo to 0.5 in grid cells where any snow was present. Photolysis rates continue to be interpolated within the range of five preset albedos in the input photolysis rates file.

The new albedo treatment is based on literature describing the evolution of snow albedo in the WRF/NOAH land surface model (LSM) over the past decade (Ek et al., 2003; Wang and Zeng, 2010; Livneh et al., 2010; and Barlage et al., 2010). Fractional snow cover (f_s) is calculated by the NOAH LSM to account for the effects of surface roughness elements (shrubs, trees, rocks and other structures) extending above thin/patchy snow:

$$f_s = 1 - \exp\left(-\alpha \frac{W}{W_c}\right) + \frac{W}{W_c}\exp(-\alpha) \quad (1)$$

where α = 2.6, W is SWE, and W_c is the threshold SWE above which f_s = 100%. In original NOAH versions, W_c was set to 0.04 m for low vegetation (grass/shrub) and to 0.08 m for tall vegetation (forest). A recent update in which these values are changed to 0.01 m and 0.2 m, respectively, has improved albedo and snow cover/duration predictions across the US (Wang and Zeng, 2010; Linveh et al., 2010). We map WRF's current values of W_c to all CAMx landuse types, except we assign a value of 0.02 m for range, mixed agriculture/range, and shrub lands where low vegetation is typically much higher than grasses. Since fractional snow cover depends on the ratio W/W_c, snow depth and SWE can be used interchangeably to represent W. Throughout CAMx we apply a common approximation that snow depth is 10×SWE. Figure 2-1 shows the relationship between f_s and snow depth for low and tall vegetation.

Snow albedo in WRF/NOAH was originally set according to vegetation type (Chen and Dudhia, 2001). Thus, only the variability in SWE (snow depth) modified the net grid cell albedo and only when SWE decreased to below the threshold value (f_s < 1). The effect of snow age (e.g., optical effects of melting and accumulation of dirt/soot) was not considered. Linveh et al. (2010) tested an albedo decay parameterization and found additional improvements in albedo and snow cover/duration predictions across the US. The form of snow albedo decay is expressed by:

$$a_s = a_{max} A^{t^B} \quad (2)$$

were a_{max} is the maximum fresh snow albedo, t is the number of days since the last snowfall, A = 0.94 (0.82) and B = 0.58 (0.46) during the accumulation (ablation) phase. Accumulation occurs during cold periods when surface temperature is below 273 K, whereas ablation occurs

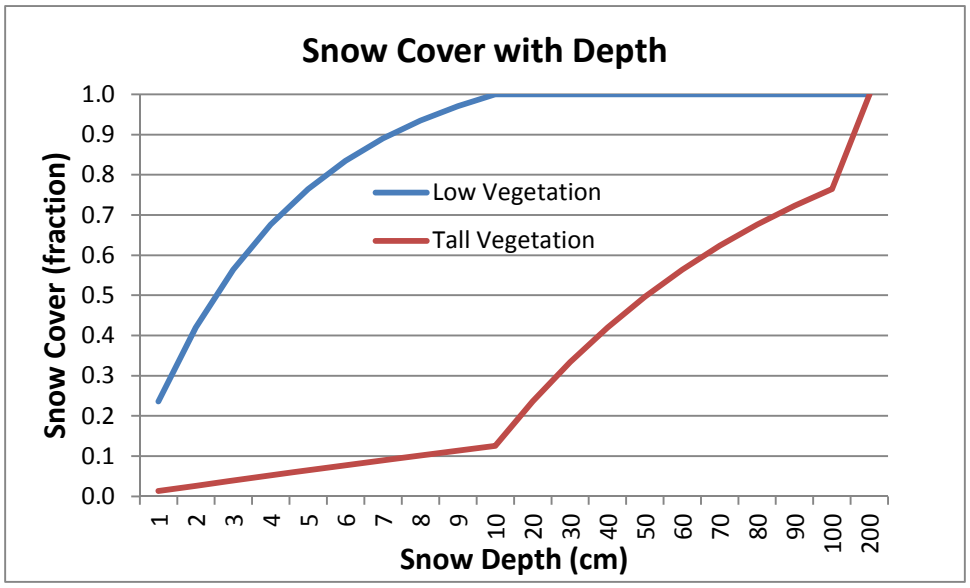

Figure 2-1. Relationship between snow cover fraction and snow depth for low (Wc = 0.01 m) and tall (Wc = 0.2 m) vegetation according to Equation 1 and the updates made by Wang and Zeng (2010) and Linveh et al. (2010).

during melting periods when surface temperature is at 273K. Snow albedo is constrained to a lower bound of 0.4. Livneh et al. (2010) set a_{max} to the average of satellite-based maximum snow albedo from Robinson and Kukla (1985) and maximum albedo from the U.S. Army Corps of Engineers (1956). A more recent modification (Barlage et al., 2010) found the best improvements in snow albedo and cover/duration at SNOTEL sites throughout the Rocky Mountains of Colorado when the maximum albedo was set to the value of 0.85 from Wiscombe and Warren (1980).

We have included the Linveh et al. (2010) formulation in CAMx, including the lower bound of 0.4 and the upper bound of 0.85. CAMx refreshes snow age to zero (and snow albedo to 0.85) when SWE accumulates by more than 0.001 m/hr (accumulating snow depth > 1 cm/hr). Figure 2-2 shows the resulting relationship between a_s and snow age during accumulation and ablation periods. The resultant grid-cell average surface albedo (a) is a linear combination of snow albedo (a_s) and terrestrial (non-snow) albedo (a_t):

$$a = f_s a_s + (1 - f_s) a_t \tag{3a}$$

where a_t is defined according to landuse type (ENVIRON, 2014). In the case where a distribution of multiple landuse types exists within a given grid cell, a linear weighting scheme is employed to account for variable snow cover fractions for each individual landuse type:

$$a = \sum_n f_n \times \{f_s(n) a_s(n) + [1 - f_s(n)] a_t(n)\} \tag{3b}$$

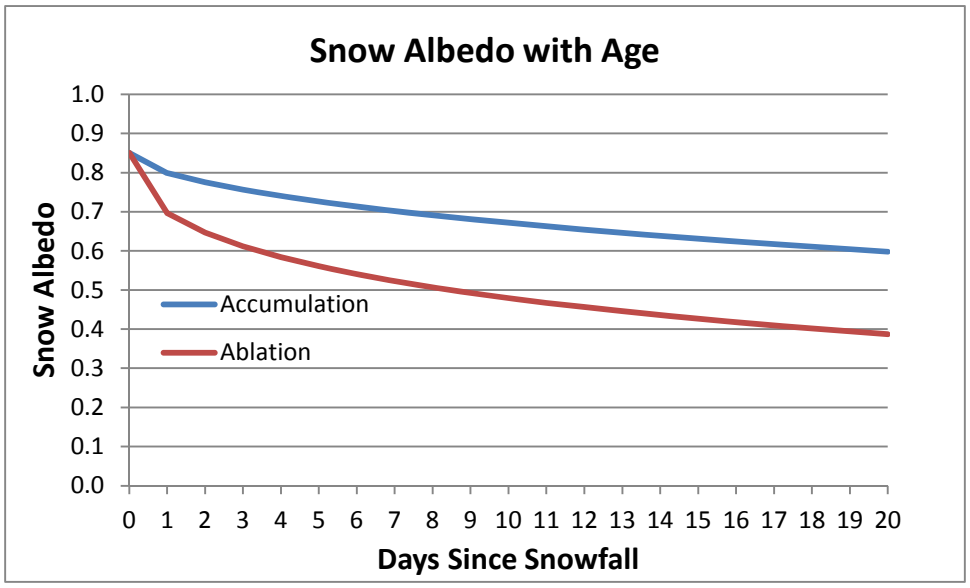

Figure 2-2. Relationship between snow albedo and snow age during accumulation and ablation periods according to Equation 2 (Linveh et al., 2010; Barlage et al., 2010).

where the sum is over all landuse types, f_n is the fractional coverage of landuse n, $a_t(n)$ is the default terrestrial albedo for landuse n, $f_s(n)$ is the fractional snow cover for landuse n, and $a_s(n)$ is the calculated snow albedo for landuse n. Figure 2-3 shows an example of grid-cell albedo evolution for a hypothetical 20-day springtime snow event (assuming ablation conditions) for low and tall vegetation grid cells with a terrestrial (non-snow) albedo of 0.05. Several snow accumulation events are specified to occur over the first 12 days, followed by rapid melting to zero depth by day 20. While total albedo increases to peak values of 0.85 quite rapidly for low-vegetation, the value for tall vegetation lags and peaks just above 0.5 at maximum snow depth. Both cases indicate effects from snow depth (fractional snow cover) and snow age.

The WRFCAMx interface program reads gridded SWE from WRF output files and passes it to CAMx; if SWE is not available on WRF output, WRFCAMx will stop with an error message. Information on snow age is not available from WRF, so WRFCAMx includes a gridded snow age counter that it also passes to CAMx. The snow clock is started at the first hour of the first CAMx simulation day, keeping in mind that CAMx spin-up periods of several to tens of days are typical. Since snow age for preexisting snow cover at the start of a run is unknown, the user must specify an initial age (e.g., 0 days, a_s = 0.85; or 5 days, a_s = 0.56-0.73 depending on surface temperature). WRFCAMx then remembers snow age values for each grid cell as it processes data for each succeeding CAMx day, resetting snow age to zero whenever SWE accumulates by more than 0.001 m/hr (snow depth > 1 cm/hr) in a particular grid cell. At the end of each WRFCAMx run, a simple file is written that contains the gridded snow age field for use in restarting a successive WRFCAMx run. The snow clock is thus continuous for all consecutively-processed CAMx days, and bridges all re-initialized WRF runs without resetting. The snow clock

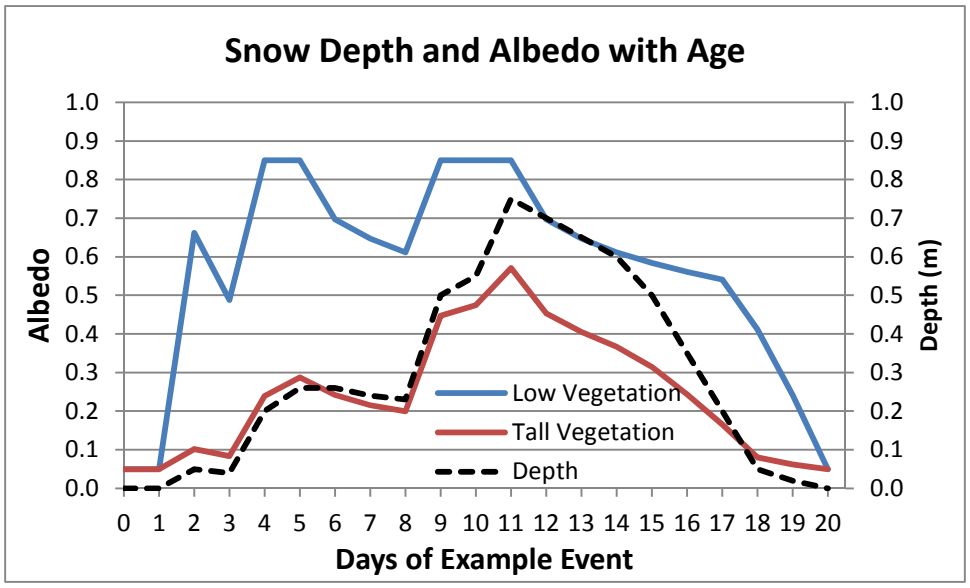

Figure 2-3. Example of grid-cell albedo evolution for a hypothetical 20-day springtime snow event (assuming ablation conditions) for low and tall vegetation grid cells with a terrestrial (non-snow) albedo of 0.05. The original model set snow albedo to 0.5 whenever any snow was present.

is reset to the user-defined value (with a warning message) any time WRFCAMx is not supplied with a previous snow age file.

The snow albedo update is also extended to the external TUV photolysis rates pre-processor. Originally, the surface albedo dimension of the photolysis lookup table contained five bins; two for the snow-free range (0.04 and 0.08) and three that represent snow cover (0.2, 0.5 and 0.8). Given that a mix of terrestrial and snow albedos is now possible, these bin definitions are modified to provide photolysis rate calculations over a wider albedo range. The new definition is 0.04, 0.1, 0.2, 0.5, and 0.9.

2.1.2 Dry Deposition

We have reinstated the original treatment of snow cover in the Zhang dry deposition algorithm by tying into the snow updates described above, thereby allowing for a range of snow cover for each of the 26 Zhang land cover categories. Specifically, the original 80% snow cover assumption in CAMx v6.1 has been reverted back to the Zhang (2003) treatment whereby snow cover fraction is determined by the ratio of grid-cell snow depth to landuse-dependent maximum snow depth. Maximum snow depth values in the Zhang module have been aligned with the W_c values described for Equation 1 to ensure consistency.

2.1.3 Surface Chemistry Module

We have extended the surface chemistry model to work with the Zhang dry deposition option and to add snow cover to the original soil and vegetation compartments. A third set of surface

chemical sorption, reaction and loss rates have been implemented to represent these processes on and within the snowpack. Details of the enhanced surface model are presented below.

The surface chemistry model treats the chemical degradation and/or transformation of deposited pollutant mass on soil, vegetation and an overlying snowpack; volatilization of chemical products back into the air (re-emission); and loss from leaching into soil, penetration into plant tissue, and uptake into snow melt water. The surface model treats any subset of species listed in the core model's chemical mechanism. Limitations of the current implementation include:

- The surface model cannot be used with the Plume-in-Grid treatment;
- Deposition to water surfaces is assumed to be irreversible and thus is not tracked by the surface model;
- Wet deposition does not contribute to surface mass, as compounds in aqueous solution are assumed to be immediately lost to surface water processes (absorption, runoff, etc.).

Figure 2-4 displays the surface model processes schematically and Table 2-1 defines parameters that are referred to in Figure 2-4. After the calculation of deposition to a snow-free surface grid cell each time step, newly deposited mass increments are divided among soil and vegetation compartments and added to total surface mass in each compartment accumulated during the model run. The net soil/vegetation split for a given grid cell is determined by the combination of the fractional coverage of each landuse type in that cell and landuse-specific split factors. The fractional coverage of 11 (Wesely) or 26 (Zhang) landuse categories in each grid cell is an external input to CAMx. The soil/vegetation splits assigned to each landuse category are internally defined within CAMx and assumed to be seasonally constant. Values for soil/vegetation splits are estimated based on simple conceptual considerations of the amount of annual-averaged vegetation (i.e., leaf area index) typical of each category (Table 2-2).

Snow is activated in the surface model when snow depth is sufficiently deep to cover exposed soil. We set that lower limit to 10 cm to be consistent with the NOAH LSM approach described above in which a 10 cm depth completely covers low-vegetation landuse. In such cases, the soil/vegetation split is replaced by the snow cover fraction such that the soil fraction is entirely snow-covered and the vegetation fraction is progressively covered with deeper snow depth (via Equation 1). The soil compartment transitions to a snow compartment; sorption coefficients and rates for chemistry and loss covert to the values set for snow (as described below). With very deep snow exceeding 200 cm, high vegetation is completely covered and the surface model reduces to a single compartment for snow.

The surface model uses partitioning (equilibrium) coefficients to calculate the amount of accumulated material sorbed to soil/snow and vegetation. The sorbed fraction is subject to chemical reactions and physical removal associated with soil leaching, plant penetration, and snow melt. The un-sorbed fraction is available for re-emission. Separate chemical-specific soil-air, vegetation-air, and snow-air partitioning coefficients are set in the CAMx chemistry

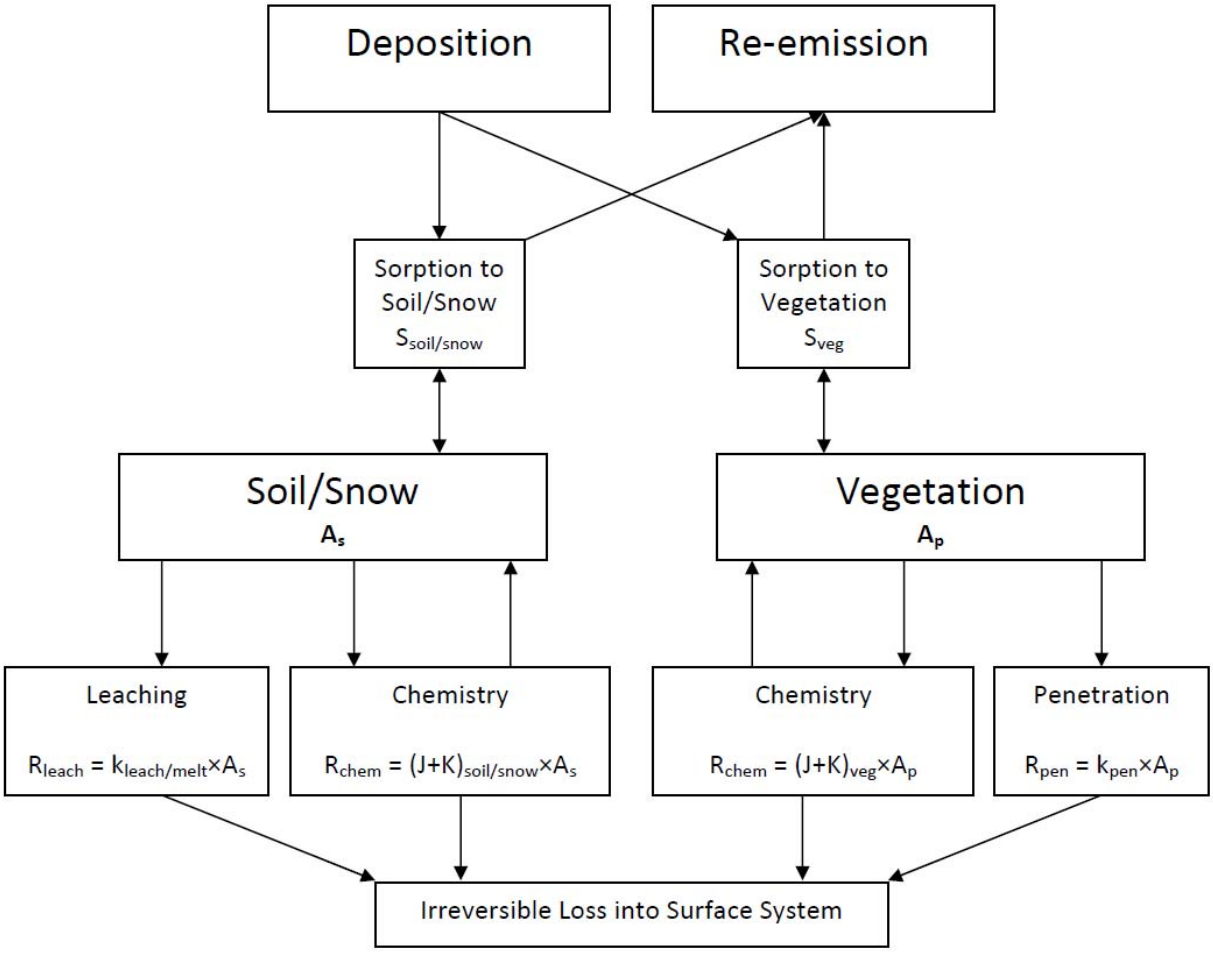

Figure 2-4. Schematic of the CAMx surface model.

parameters file. They represent the equilibrium ratio of chemical on a surface to chemical in air at the air-surface interface. For example, a compound with a partitioning coefficient of 10,000 (unitless) has an equilibrium concentration on the surface that is 10,000 times more than that in air. Chemistry can simply decay deposited material as a removal process, or it can generate products that can subsequently re-emit depending on the products' partitioning coefficient. All surface removal processes are assumed to be irreversible and result in a permanent removal of mass. Chemistry, soil leaching, plant penetration, and snow melt loss are dependent on chemical properties of the compounds and also on numerous site-specific factors such as soil, vegetation, and snow properties, highly transient meteorological conditions, etc. Often these factors are unknown or fall within a range. The rates of these processes are defined as the process rate coefficient (k) times the mass on the surface area, or areic mass (A):

$$R_{process} = k_{process} \times A_{surface} \quad (4)$$

Table 2-1. Description of CAMx surface model variables shown in Figure 2-4.

Variable	Definition	Units
A_s	Areic mass of compound on soil or snow	mol ha^{-1}
A_p	Areic mass of compound on vegetation	mol ha^{-1}
S_{soil}	Soil-air partitioning coefficient	unitless
S_{snow}	Snow-air partitioning coefficient	unitless
S_{veg}	Vegetation-air partitioning coefficient	unitless
k_{leach}	Soil leaching rate coefficient	min^{-1}
K_{melt}	Snow melt loss rate coefficient	min^{-1}
k_{pen}	Leaf penetration rate coefficient	min^{-1}
J	Photolysis chemistry rate coefficient	min^{-1}
K	Heterogeneous chemistry rate coefficient	min^{-1}
R_{leach}	Leaching or snow melt loss rate	mol ha^{-1} min^{-1}
R_{pen}	Leaf penetration rate	mol ha^{-1} min^{-1}
R_{chem}	Chemistry rate	mol ha^{-1} min^{-1}

Table 2-2(a). Wesely landuse categories and associated annual-averaged soil/vegetation split factors, UV albedo, and SWE W_c.

Category Number	Land Cover Category	Surface Parameters		
		Soil Fraction	UV Albedo	Snow W_c (m SWE)
1	Urban	0.7	0.08	0.2
2	Agricultural	0.2	0.05	0.01
3	Rangeland	0.5	0.05	0.02
4	Deciduous forest	0.1	0.05	0.2
5	Coniferous forest, wetland	0.1	0.05	0.2
6	Mixed forest*	0.1	0.05	0.2
7	Water	n/a	0.04	n/a
8	Barren land	1.0	0.08	0.01
9	Non-forested wetlands	0.2	0.05	0.01
10	Mixed agricultural/range*	0.3	0.05	0.02
11	Rocky (with low shrubs)	0.5	0.05	0.01

Table 2-2(b). Zhang landuse categories and associated annual-averaged soil/vegetation split factors, UV albedo, and SWE W_c.

Category Number	Land Cover Category	Surface Parameters		
		Soil Fraction	UV Albedo	Snow W_c (m SWE)
1	Water	n/a	0.04	n/a
2	Ice	n/a	0.5	0.01
3	Inland lake	n/a	0.04	n/a
4	Evergreen needleleaf trees	0.1	0.05	0.2
5	Evergreen broadleaf trees	0.1	0.05	0.2
6	Deciduous needleleaf trees	0.1	0.05	0.2
7	Deciduous broadleaf trees	0.1	0.05	0.2
8	Tropical broadleaf trees	0.1	0.05	0.2
9	Drought deciduous trees	0.1	0.05	0.2
10	Evergreen broadleaf shrubs	0.5	0.05	0.03
11	Deciduous shrubs	0.5	0.05	0.02
12	Thorn shrubs	0.5	0.05	0.03
13	Short grass and forbs	0.5	0.05	0.01
14	Long grass	0.3	0.05	0.02
15	Crops	0.2	0.05	0.01
16	Rice	0.2	0.05	0.01
17	Sugar	0.2	0.05	0.01
18	Maize	0.2	0.05	0.01
19	Cotton	0.2	0.05	0.01
20	Irrigated crops	0.2	0.05	0.01
21	Urban	0.7	0.08	0.2
22	Tundra	0.2	0.05	0.01
23	Swamp	0.2	0.05	0.01
24	Desert	1.0	0.08	0.01
25	Mixed wood forest	0.1	0.05	0.2
26	Transitional forest	0.1	0.05	0.2

When the actual rate coefficients (or inversely, the half-lives, $t_{½}$) are unknown for the substance, they can be generalized by 5 classes:

1. Very fast: $t_{½}$ = 0.04 d k = 17 d^{-1} = 1.2×10-2 min^{-1}
2. Fast: $t_{½}$ = 0.21 d k = 3.3 d^{-1} = 2.3×10-3 min^{-1}
3. Moderate: $t_{½}$ = 1.0 d k = 0.69 d^{-1} = 4.8×10-4 min^{-1}
4. Slow: $t_{½}$ = 5.0 d k = 0.14 d^{-1} = 9.7×10-5 min^{-1}
5. Very slow: $t_{½}$ = 25 d k = 0.03 d^{-1} = 2.1×10-5 min^{-1}

A 6th class can be added by setting the k-value to zero or a de minimis value to effectively remove the process from consideration. In this manner chemicals can be modeled with an estimated half-life that is unique for each process.

Note that all partitioning coefficients and rates other than photolysis are fixed and ignore dependence on various environmental conditions (e.g., temperature, pressure, surface type, surface moisture, etc.). Photolysis rates are specified by the user to represent peak direct-exposure clear-sky values at zero zenith (solar noon) and are internally adjusted for solar angle, cloud attenuation (as calculated for atmospheric photolysis), and shade effects using multiplicative factors. Shade effects are arbitrarily defined in the current implementation.

A multiplicative "shade factor" is defined to reduce photolysis rates within/below vegetation. For snow-free cells, the shade factor for vegetation is set to 0.5 while the shade factor for soil is defined by the soil/vegetation fraction (e.g., 1.0 for barren land, 0.1 for forests; see Table 2-2). Snow cover reduces shading effects (increases shade factors) to account for enhanced internal UV scattering within the snowpack. The product of snow fraction and snow albedo is added to the snow-free shade factors for vegetation and soil. This can increase the shade factor to over 1 depending on the circumstances. For example, barren lands that are entirely covered by snow with an albedo of 0.85 have a net soil/snow shade factor of 1.0 + 1.0×0.85 = 1.85, which enhances clear-sky photolysis in the snowpack by 85%. Forests that are 20% covered by snow with the same albedo have a net soil/snow shade factor of 0.1 + 0.2×0.85 = 0.27, and a vegetative shade factor of 0.5 + 0.2*0.85 = 0.67. In this case, clear-sky photolysis rates that were originally reduced to 10% and 50% on soil and in the canopy, respectively, are reduced to 27% and 67% in the presence of 20% snow cover.

Losses by soil leaching, plant penetration, and snow melt are arbitrarily accelerated during rain events, such that a 1 mm/hr rainfall rate results in an e-folding loss of surface mass in 1 hour. Mass loss within the snowpack by melting alone occurs only when surface temperature is at 273 K. Snowpack loss also occurs during snowfall such that a 1 cm/hr accumulation results in an e-folding loss of surface mass in 24 hours by successively burying pollutant mass and limiting its ability to diffuse through the snowpack. The model assumes that no surface mass is re-introduced as snow depth/fraction decrease during sublimation or melting (i.e., we continue to assume irreversible loss of surface mass as implemented for soil and vegetation).

The approach for re-emission of volatilized (un-sorbed) mass is consistent with the CAMx dry deposition algorithm. Since water surfaces are not considered by the surface model, re-emission fluxes from water are ignored in this implementation. Dry deposition of material from the lowest model layer to the surface is treated as an irreversible (fully sorbed) first-order flux through the use of a dry deposition velocity. Re-emission of volatilized (un-sorbed) mass is also treated as a first-order 1-way flux using an "effective" velocity that is similar in form to deposition:

$$v_e = \frac{1}{r_a + r_b} \quad (5)$$

where r_a is the aerodynamic resistance to turbulent transfer through the lowest model layer, and r_b is the resistance to molecular diffusion through the laminar sub-layer in contact with surface elements. The deposition surface resistance term r_s is missing since only the pre-determined un-sorbed fraction of surface mass is considered for surface-to-air transfer. The r_a and r_b terms are calculated by the surface model in exactly the same manner as the values used for dry deposition to ensure consistency.

2.1.3.1 Running CAMx With the Surface Model

The CAMx surface model parameters that need to be specified for each compound or surface reaction to be tracked are as follows:

S_{soil}	Soil-air partitioning coefficient	unitless
S_{veg}	Vegetation-air partitioning coefficient	unitless
S_{snow}	Snow-air partitioning coefficient	unitless
k_{leach}	Soil leaching rate coefficient	min^{-1}
k_{pen}	Leaf penetration rate coefficient	min^{-1}
k_{melt}	Snow melt loss rate coefficient	min^{-1}
J_{soil}	Soil photolysis rate coefficient	min^{-1}
K_{soil}	Soil heterogeneous chemistry rate coefficient	min^{-1}
J_{veg}	Vegetation photolysis rate coefficient	min^{-1}
K_{veg}	Vegetation heterogeneous chemistry rate coefficient	min^{-1}
J_{snow}	Snow photolysis rate coefficient	min^{-1}
K_{snow}	Snow heterogeneous chemistry rate coefficient	min^{-1}

These values are set at the end of the CAMx chemistry parameters file; an example of the chemistry parameters file format is shown in Figure 2-5. A control record is also needed at the top of the chemistry parameters file to define the number of species and reactions to track.

A CAMx namelist control file variable called "SURFACE_MODEL" must be set to "true" in order to invoke the surface model. When the surface model is invoked, the surface model section of

```
CAMx Version       |VERSION6.1
Mechanism ID       |2
Aerosol Option     |NONE
Description        |CB6r2 (r98/30/13 version) + ECH4
No of gas species  |75
No of aero species |0
No of reactions    |216
Prim photo rxns    |23 1 8 9 21 27 28 38 43 47 50 56 88 92 97 98 108 112 114 117
 119 128 129 161
No of sec photo rxn|6
ID, prim ID, scale |64  56 1.0
                   |90  88 1.0
                   |163 1  0.07
                   |196 1  0.015
                   |197 1  0.08
                   |201 1  0.08
SrfMod #spc, #rxns |3 2
.
.
.
Surface Model
Species          SoilSorb SoilLeach   VegSorb    VegPen   SnoSorb    SnoMlt
  1  HNO3        1.00E+10  1.00E-10  1.00E+10  1.00E-10  1.00E+10  9.70E-05
  2  PNA         1.00E+10  1.00E-10  1.00E+10  1.00E-10  1.00E+10  9.70E-05
  3  HONO        1.00E+00  1.00E-10  1.00E+00  1.00E-10  1.00E+00  9.70E-05
Rxn  Precursor Product       Soil K    Soil J     Veg K     Veg J    Snow K    Snow J
  1  HNO3      HONO        0.00E+00  0.00E+00  0.00E+00  0.00E+00  0.00E+00  1.00E-03
  2  PNA       HONO        0.00E+00  0.00E+00  0.00E+00  0.00E+00  1.00E-01  0.00E+00
```

Figure 2-5. The portions of the CAMx chemistry parameters file (highlighted) to support the surface model. In this example, 3 gases are treated, where nitric acid (HNO_3) and peroxynitric acid (PNA) react to form nitrous acid (HONO). All three are subject to decay by soil leaching, plant penetration, and snow melt loss. The values shown here are for illustrative purposes only and do not represent any known surface chemistry mechanism.

the chemistry parameters file is read and the respective equilibrium and rate variables are set accordingly.

2.2 Winter Chemistry

Alkyl nitrates ($RONO_2$) are formed when alkanes are oxidized in the atmosphere in the presence of nitric oxide (NO). Alkanes are compounds of hydrogen and carbon with only single bonds connecting the atoms, e.g., methane (CH_4), ethane (C_2H_6), propane (C_4H_8), etc. Analysis of air samples collected during the 2013 Uinta Basin Ozone Study (UBOS) shows that alkanes dominated the organic gases present in the air. The composition shown in Figure 2-6 resembles natural gas with methane the largest contributor by mass and contributions of other alkanes decreasing with increasing size (ethane > propane > butanes > pentanes > hexane). Methanol is the only compound named in Figure 2-6 that is not an alkane, and not a constituent of natural gas; methanol is used as an anti-freeze by the oil and gas industry in the Uinta Basin (Stoeckenius, 2015).

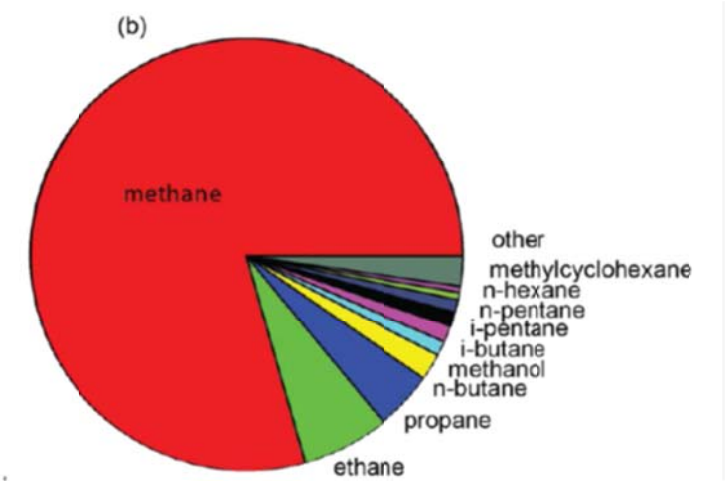

Figure 2-6. Organic gas contributors sorted by mass during UBOS 2013 (Figure 5-13b from http://www.deq.utah.gov/locations/U/uintahbasin/docs/2014/03Mar/UBOS-2013-Final-Report/UBOS_2013_SynthesisReport_Sec5_Horsepool.pdf).

The formation of alkyl nitrates from alkanes can be described by the following reactions in which an alkane (RH) reacts with hydroxyl radical ($HO^{\bullet}$)[1] and oxygen (O_2) to form an alkyl peroxy radical ($RO_2^{\bullet}$) that has two potential reaction pathways with $NO^{\bullet}$:

1) $HO^{\bullet} + RH \rightarrow R^{\bullet} + H_2O$
2) $R^{\bullet} + O_2 \rightarrow RO_2^{\bullet}$
3a) $RO_2^{\bullet} + NO^{\bullet} \rightarrow RONO_2$
3b) $\rightarrow RO^{\bullet} + NO_2^{\bullet}$

Perring et al. (2013) have reviewed the atmospheric impacts of alkyl nitrate formation. The yield of alkyl nitrate is determined by the branching ratio for reactions 3a and 3b, which depends on both temperature and pressure (Atkinson et al., 1983). The association reaction of RO_2 with NO in reaction 3a is favored over reaction 3b at lower temperatures and higher pressures. Alkyl nitrate formation can influence ozone production because both NO and radicals are terminated by alkyl nitrate formation. Lee et al. (2014) considered how cold winter conditions in the Uinta Basin will affect reactions 3a and 3b and concluded (without conducting ozone modeling) that omitting the temperature dependence of reactions 3a and 3b may cause 15% high bias in ozone formation. Photochemical grid modeling is needed to provide a more definitive evaluation of this question.

The temperature dependence of reactions 3a and 3b is omitted from current versions of the chemical mechanisms used in photochemical grid models, i.e., CB05-TU (Whitten et al., 2010),

[1] The dot signifies that hydroxyl (HO) is a radical, i.e., has one unpaired electron. Note that NO and NO_2 also are radicals. O_2 is a di-radical.

CB6 (Hildebrandt Ruiz and Yarwood, 2013), SAPRC11 (Carter and Heo, 2013) and RACM2 (Goliff et al., 2013) and also from the explicit Master Chemical Mechanism (http://mcm.leeds.ac.uk/MCM/).

Atkinson et al. (1983) presented equations to describe the temperature and pressure dependence of alkyl nitrate yield [*k3a*/(*k3a*+*k3b*)] from the branching ratio (*k3a*/*k3b*), where *k3a* is the rate constant for reaction 3a. These equations have been updated several times by the authors with the most recent version appearing in Arey et al. (2001):

$$\frac{k3a}{k3b} = \left(\frac{Y_0^{298}[M](T/298)^{-m_0}}{1 + \frac{Y_0^{298}[M](T/298)^{-m_0}}{Y_\infty^{298}(T/298)^{-m_\infty}}} \right) F^Z \quad (6a)$$

$$Z = \left[1 + \left(\log\left(\frac{Y_0^{298}[M](T/298)^{-m_0}}{Y_\infty^{298}(T/298)^{-m_\infty}} \right) \right)^2 \right]^{-1} \quad (6b)$$

$$Y_0^{298} = \alpha e^{\beta n} \quad (6c)$$

where Y_o^{298} is the low-pressure limit of the rate constant ratio *k3a*/*k3b*, Y_∞^{298} is the high-pressure limit of *k3a*/*k3b*, [*M*] is the atmospheric density (molecule cm^{-3}) at temperature *T* (K), and *n* is the number of carbon atoms in the alkane. Parameters in the expression have the following values: $\alpha = 2\times10^{-22}$ cm^3 molecule^{-1}, $\beta = 1.0$, $Y_\infty^{298} = 0.43$, $F = 0.41$, $m_0 = 0$ and $m_\infty = 8$. Recent experimental data of Yeh and Ziemann (2014) confirm the expression of Arey et al. (2001) for n-alkanes containing 3 to 14 carbon atoms.

Figure 2-7 shows the branching ratio for alkyl nitrate formation [*k3a*/(*k3a*+*k3b*)] from n-alkanes with 3 to 14 carbon atoms (propane to tetradecane) at 298 K and 1 atmosphere. The alkyl nitrate branching ratio increases with carbon number and asymptotes toward 0.3 for alkanes larger than tetradecane. Alkyl nitrate branching ratios are low for alkanes smaller than propane, about 0.01 for ethane and essentially zero for methane.

Figure 2-8 shows the branching ratio for alkyl nitrate formation from pentane at different temperatures and pressures. Representative winter conditions in the Uinta basin (260 K and 0.85 atm) differ from typical laboratory conditions (298 K and 1 atm). For pentane, decreasing temperature from 298 K to 260 K increases alkyl nitrate formation by 64% whereas decreasing pressure from 1 atm to 0.85 atm decreases alkyl nitrate formation by 7% for a combined (multiplicative) increase of 54%. Increases in alkyl nitrate formation from room temperature to Uinta Basin winter conditions for various alkanes range from 29% to 95% as shown in Table 2-3. Also listed in Table 2-3 are the model species that represent alkanes in revision 2 of the Carbon Bond 6 mechanism (CB6r2; Hildebrandt Ruiz and Yarwood, 2013). Emissions of methane,

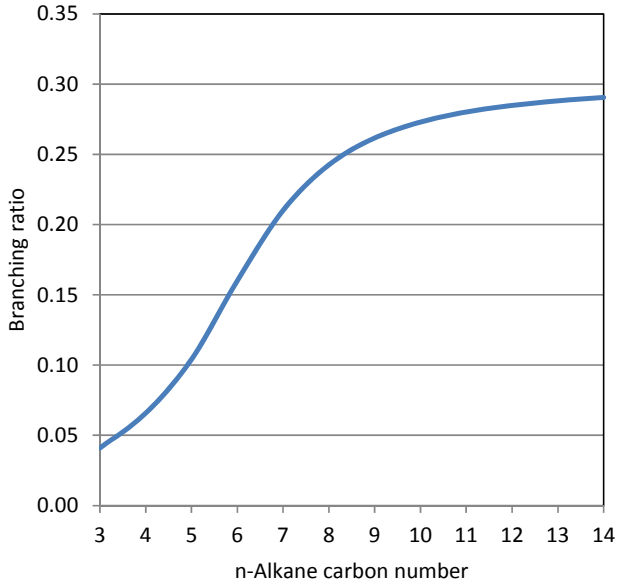

Figure 2-7. Branching ratio for alkyl nitrate formation [*k3a*/(*k3a+k3b*)] from n-alkanes computed at 298 K and 1 atmosphere (Arey et al., 2001).

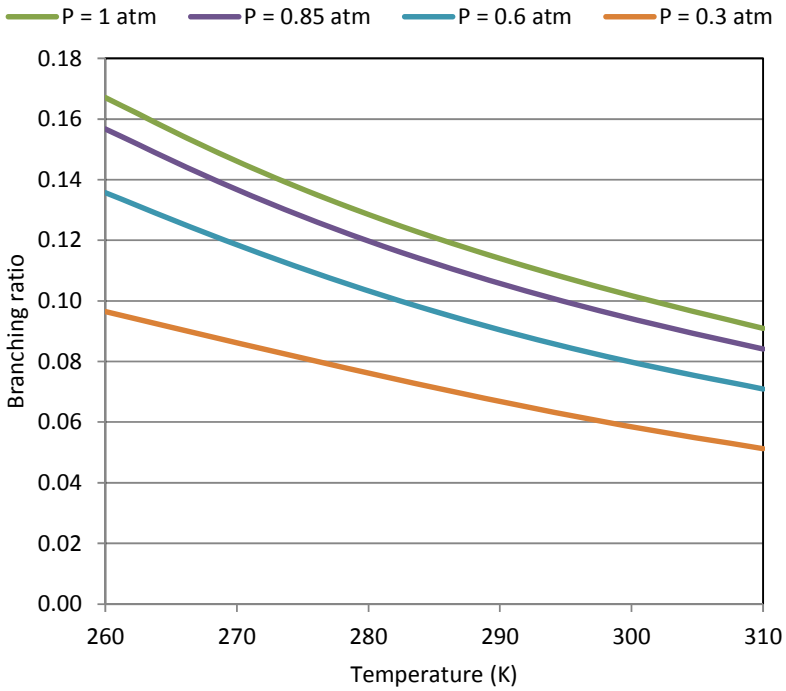

Figure 2-8. Branching ratio for alkyl nitrate formation [*k3a*/(*k3a+k3b*)] from pentane computed at different temperatures and pressures (Arey et al., 2001).

Table 2-3. Percent increase in alkyl nitrate branching ratio from room temperature to Uinta Basin winter conditions for various alkanes.

Alkane	Carbon Number	Percent increase[1]	Represented in CB6r2 by
Methane	1	N/A[2]	ECH4
Ethane	2	N/A[3]	ETHA
Propane	3	29	PRPA
Butane	4	54	PAR
Pentane	5	54	PAR
Hexane	6	49	PAR
Heptane	7	65	PAR
Octane	8	82	PAR
Decane	10	93	PAR
Tetradecane	14	95	PAR

Notes:
1. Change computed using expression of Arey et al. (2001) from conditions of 298 K and 1 atm to 260 K and 0.85 atm.
2. Temperature dependence not considered because the alkyl nitrate branching ratio for methane is near zero
3. Temperature dependence not considered because the alkyl nitrate branching ratio for ethane is <1%

ethane and propane are each represented by the explicit species ECH4, ETHA and PRPA, respectively, whereas larger alkanes are represented by the lumped species PAR.

Because the alkanes represented by PAR (butane and larger) have varying temperature and pressure dependencies (Table 2-3) those dependence assigned to PAR should correspond reasonably well to the alkanes that are important in the Uinta Basin. Figure 2-6 shows that methane dominates air concentrations of organic gasses on a mass basis, but methane also reacts very slowly in the atmosphere (lifetime of ~10 years) meaning that most methane emitted in the Uinta Basin leaves the basin without reacting. Weighting organic gas concentrations from Figure 2-6 by their rate constants for reacting with OH (called OH reactivity) indicates which species are most likely to participate in ozone formation within the Uinta Basin (Figure 2-9). Considering the alkanes represented by PAR, those with 4 to 7 carbon atoms dominate OH reactivity indicating that the data for pentane shown in Figure 2-8 may be considered representative for alkanes in the Uinta Basin.

The formation of alkyl nitrates from PRPA and PAR in CB6r2 is determined by the reactions show in Table 2-4 as Scheme 1 (Hildebrandt Ruiz and Yarwood, 2013). Alkyl nitrates (NTR1 and NTR2) are formed when the operator XO2N reacts with NO such that the alkyl nitrate branching ratio for PAR is 13% as by the yield for XO2N of 0.13 in reaction 132. Similarly, the alkyl nitrate branching ratio for PRPA is 3% as determined by the yield for XO2N of 0.03 in reaction 131.

We have developed the CB6r3 chemical mechanism from CB6r2 to extend applicability to winter and summer conditions. The formation of alkyl nitrates from PRPA and PAR in CB6r3 is determined by the reactions shown in Table 2-5 as Scheme 2. CB6r3 (Scheme 2) was designed to produce the same alkyl nitrate yields as CB6r2 (Scheme 1) at room temperature and pressure (298 K and 1 atm). For PAR, a new operator XPAR is the sole product of revised reaction 131 and removed by two reactions numbered 131a and 131b. In Scheme 2, the alkyl nitrate

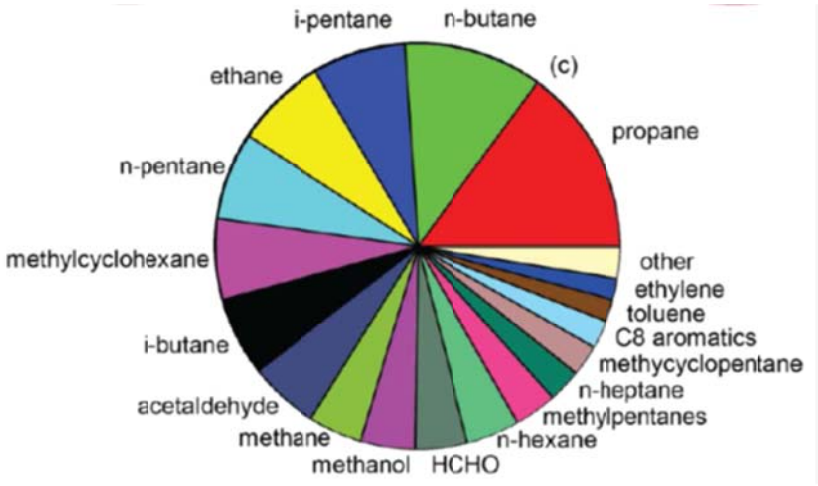

Figure 2-9. Organic gas concentrations weighted by their OH rate constants (*kOH*) during UBOS 2013 (Figure 5-13c from http://www.deq.utah.gov/locations/U/uintahbasin/docs/2014/03Mar/UBOS-2013-Final-Report/UBOS_2013_SynthesisReport_Sec5_Horsepool.pdf).

Table 2-4. Scheme 1: formation of alkyl nitrates from alkanes in CB6r2.

Reaction No.	Reaction	k_{298} (cm^3 $molecule^{-1}$ s^{-1})
131	PRPA + OH = 0.710 ACET + 0.260 ALDX + 0.260 PAR + 0.970 XO2H + 0.030 **XO2N** + RO2	1.07×10^{-12}
132	PAR + OH = 0.110 ALDX + 0.760 ROR + 0.130 **XO2N** + 0.110 XO2H + 0.760 XO2 + RO2 + -0.110 PAR	8.10×10^{-13}
83	**XO2N** + NO = 0.500 NTR1 + 0.500 NTR2	9.04×10^{-12}

Note: The CB6 specie RO2 represents the total RO2 radical concentration. Therefore, the product yield of RO2 equals the sum of the product yields of XO2 and XO2N.

Table 2-5. Scheme 2: formation of alkyl nitrates from alkanes in CB6r3.

Reaction No.	Reaction	k_{298} (cm^3 $molecule^{-1}$ s^{-1})
131	PRPA + OH = XPRP	1.07×10^{-12}
131a	XPRP = **XO2N** + RO2	3.09×10^{-2}
131b	XPRP = 0.732 ACET + 0.268 ALDX + 0.268 PAR + XO2H + RO2	1.0
132	PAR + OH = XPAR	8.10×10^{-13}
132a	XPAR = **XO2N** + RO2	1.49×10^{-1}
132b	XPAR = 0.126 ALDX + 0.874 ROR + 0.126 XO2H + 0.874 XO2 + RO2 + -0.126 PAR	1.0
83	**XO2N** + NO = 0.500 NTR1 + 0.500 NTR2	9.04×10^{-12}

branching ratio from PAR equals the rate constant ratio *k131a*/(*k131a+k131b*), which is 0.130 at 298 K and 1 atm (Table 2-6). Thus, Schemes 1 and 2 are equivalent at 298 K and 1 atm with Scheme 2 having the advantage that alkyl nitrate yields can vary with temperature and pressure by varying *k131b*, as shown in Table 2-6. In CB6r3, *k131b* is computed using the expression of Arey et al. (2001) with a carbon number of 5.5, which reproduces the alkyl nitrate yield of CB6r2 (0.130) at 298 K and 1 atm. A similar approach is implemented for PRPA using the operator XPRP. CB6r3 (Scheme 2) is suitable for representing the alkane mixture reacting in the Uinta Basin (see Figure 2-9) although the derivation of CB6r3 does not rely upon this particular mixture of alkanes.

Table 2-6. CB6r3 yields of XO2N for propane (PRPA) and larger alkanes (PAR) for conditions of room temperature and pressure (298 K, 1 atm) and the Uinta Basin in winter (260 K, 0.85 atm).

Conditions T(K), P(atm)	*k131a* (s^{-1})	*k131b* (s^{-1})	Yield of XO2N from PRPA *k131a*/(*k131a+k131b*)	*k132a* (s^{-1})	*k132b* (s^{-1})	Yield of XO2N from PAR *k132a*/(*k132a+k132b*)
298, 1	0.0309	1	0.030	0.149	1	0.130
298, 0.85	0.0277	1	0.027	0.138	1	0.121
260, 1	0.0454	1	0.043	0.270	1	0.213
260, 0.85	0.0397	1	0.038	0.249	1	0.199

A complete listing of CB6r3 is given in Appendix A. The reactions numbered 131a, 131b, 132a and 132b in Scheme 2 are numbered 217 - 220 in CB6r3.

The modifications to PAR chemistry shown in Scheme 2 could readily be adapted to CB05. The modifications for propane cannot be adapted because CB05 does not include an explicit propane species.

3.0 TESTING AND ANALYSIS

The CAMx improvements described in Section 2 have been tested using a wintertime modeling database developed by UDAQ. We first compare results from the original CAMx v6.1 against the new model with snow updates (albedo, deposition and surface model) and CB6r3 chemistry to gauge effects on ozone production in the Uinta Basin. We then describe and evaluate additional sensitivity tests with modified emissions from the oil and gas (O&G) sector in the Uinta Basin to identify needed improvements in the local emissions inventory.

Figure 3-1 shows the modeling domain with the locations of monitoring sites clustered in the Uinta Basin of Utah. The domain is represented as a three-dimensional grid with 153×156 horizontal grid cells at 4 km spacing, and 41 vertical layers spanning from the surface to a pressure altitude of 50 hPa (16-20 km above local terrain). Six vertical layers resolve the lowest 100 m with a 12 m surface layer, where the bulk of local wintertime photochemistry occurs in the Uinta Basin.

The modeling episode covers the February 1-7, 2013 UBOS period. During this stagnant, highly stable cold-pool event, ozone in the snow-covered Uinta Basin was measured to steadily rise day-to-day, peaking over 120 ppb at multiple sites on February 5.

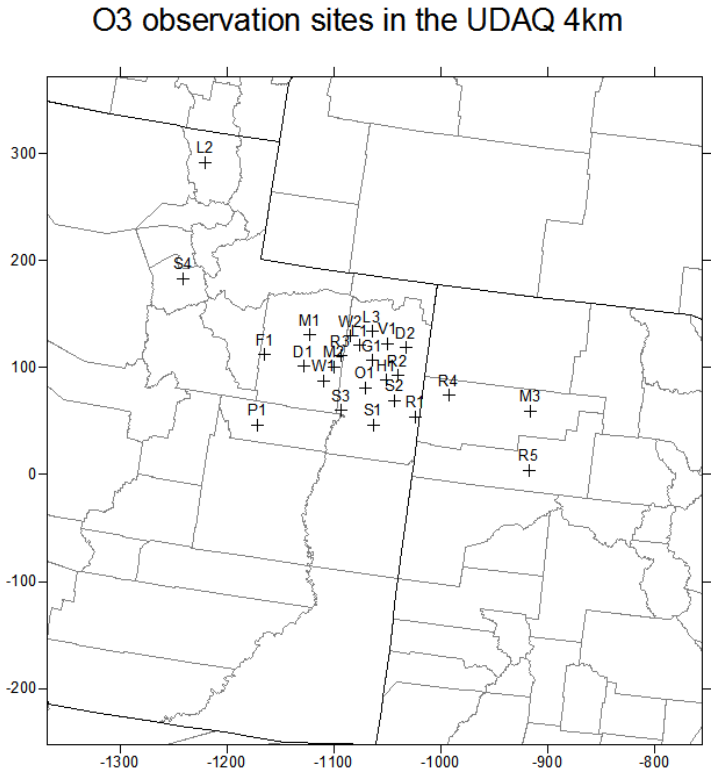

Figure 3-1. CAMx modeling domain featuring 4 km grid spacing. Locations of surface monitoring sites are noted; the cluster of sites in northeastern Utah indicates the extent of the Uinta Basin.

The datasets employed in the modeling include:

- Hourly WRF meteorological and surface variable fields developed by the University of Utah;
- Hourly, domain-wide CAMx-ready gridded and point source emissions based on UDAQ's 2010 $PM_{2.5}$ modeling along the Wasatch Front, speciated for CB05 chemistry (initial testing);
- Hourly, domain-wide CAMx-ready gridded and point source emissions based on UDAQ's 2011 National Emission Inventory (NEI) submission, speciated for CB05 chemistry (sensitivity testing);
- 6-hourly CAMx-ready gridded initial and boundary conditions extracted by UDAQ from MOZART global model output for CB05 chemistry;
- February 2013 UBOS measurement data.

3.1 Initial CAMx Testing

CAMx v6.1 was run with and without the improvements described in Section 2 for the February 2013 modeling episode. These initial tests were conducted using the 2010-based CB05 emission inventory developed by UDAQ. Tests were run incrementally: first with the unmodified model, then introducing snow albedo and deposition updates, then shifting to the new CB6r3 mechanism, then adding the updated surface chemistry model treating HONO production from deposited HNO_3 and NO_2. It is acceptable to use CB05 emissions with the CB6 chemistry mechanism because CB6 is backwards compatible, although the incremental benefits from emission speciation will not be fully realized. The surface chemistry model was configured to treat an arbitrary selection of chemical species and rates solely for the purpose of testing the code, not to suggest any real process that might occur in the Uinta Basin. Ozone enhancement from heterogeneous chemistry in the snowpack is highly speculative, and we note that there is currently no conclusive evidence for a surface chemical pathway.

Figure 3-2 shows the "baseline" (unmodified CAMx) ozone results at 2 PM MST, 5 February over the entire modeling domain. Ozone in the Uinta Basin is simulated to peak at just about 60 ppb, roughly half of the observed peak. Figure 3-3 shows the total net effect of all model updates on simulated ozone at the same time. Altogether, simulated ozone increases in the Uinta Basin by 10-20 ppb. The snow albedo/deposition update and the inclusion of arbitrary surface chemistry contribute to ozone increases. However, the introduction of CB6r3 chemistry contributes to a small (1-3 ppb) ozone reduction. This CB6r3 signal is expected as cold temperatures increase production of organic nitrate from the RO_2+NO reaction and reduce production of NO_2 and thus ultimately O_3. This also aligns with the expectation of Lee et al. (2014).

Figure 3-4 displays time series of observed and simulated ozone from the baseline and updated model at the Horsepool monitoring site in the eastern Uinta Basin. Simulated ozone is far too low in both model cases, varying between 20-50 ppb during the episode, whereas observed ozone varies between 50-120 ppb. However, simulated ozone in the background environment outside the basin is much higher and generally agrees well-with observations (Figure 3-5).

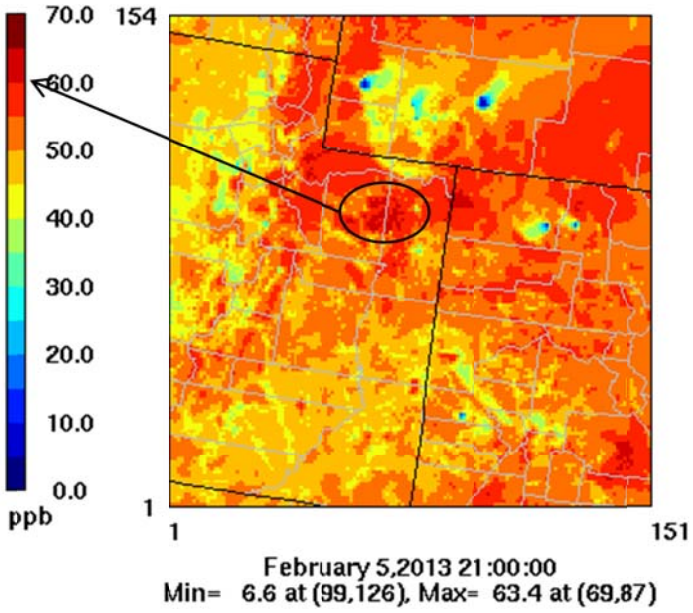

Figure 3-2. Baseline simulated ozone at 21:00 UTC (2 PM MST), February 5 over the 4 km modeling grid. These results were generated with the unmodified CAMx v6.10.

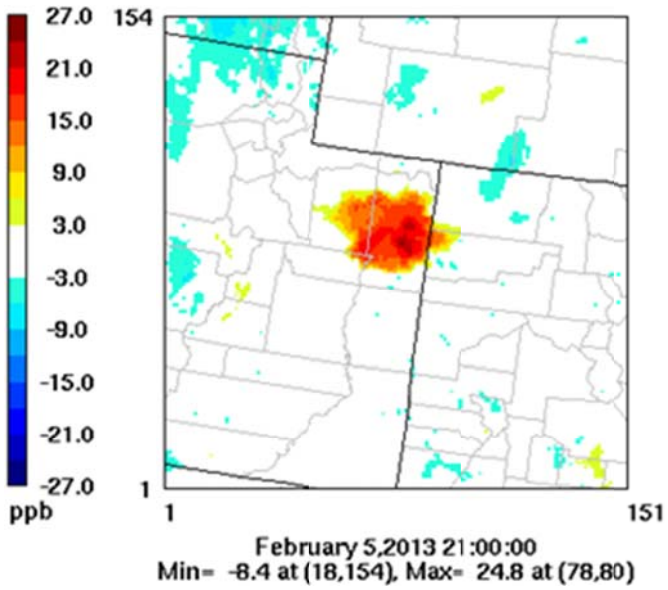

Figure 3-3. Difference in simulated ozone at 21:00 UTC (2 PM MST), Februray 5 over the 4 km modeling grid resulting from the snow albedo, dry deposition, CB6r3, and surface model updates in CAMx v.6.10.

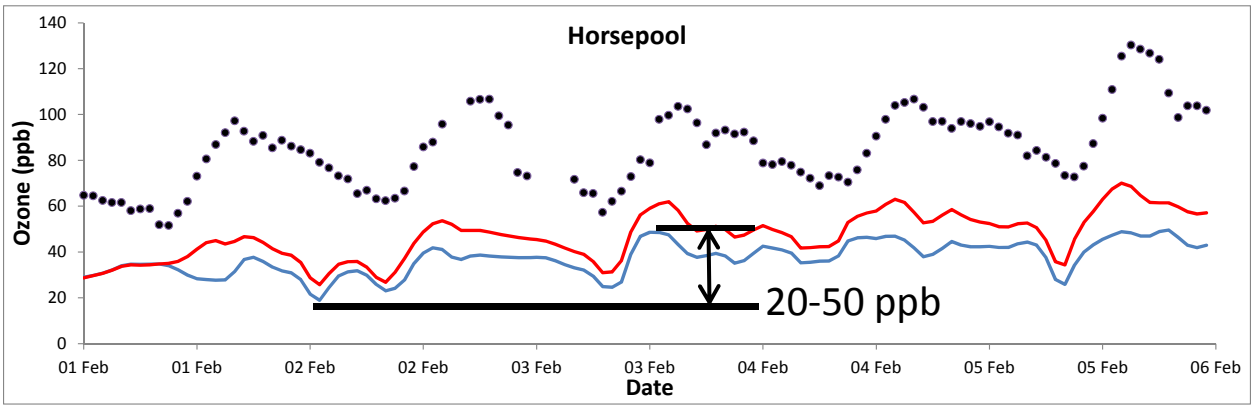

Figure 3-4. Time series of hourly observed (dots) and simulated ozone at Horsepool during February 1-5, 2013. Simulation results are shown for the baseline case (blue line) using the unmodified version of CAMx, and for the modified CAMx case (red line) with updated snow albedo, dry deposition, CB6r3, and surface model.

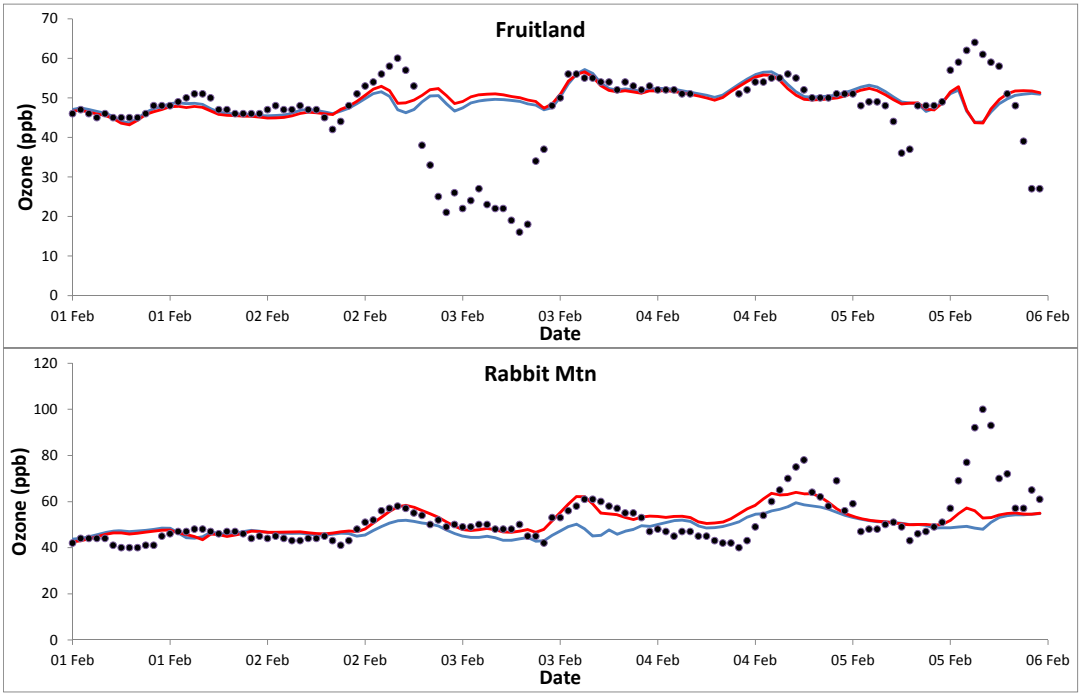

Figure 3-5. As in Figure 3-4, but at Fruitland (top) near the western rim of the Uinta Basin and Rabbit Mountain (left) near the eastern rim.

Comparisons to 2013 UBOS measurements confirm that the model is NOx-rich and VOC-poor, leading to ozone destruction and inhibited production. Therefore, the model updates alone are insufficient to simulate ozone at measured levels.

3.2 Emission Sensitivity Testing

Modeling conducted by Ahmadov et al. (2014) using WRF-Chem has achieved higher ozone by doubling VOC emissions while reducing NOx by a factor of 3. Our analysis of simulated NOx and VOC against 2013 UBOS measurements at Horsepool also indicated a similar over prediction of NOx, similar under predictions of alkanes, and much larger under predictions of aldehydes.

Subsequent to our initial modeling tests described in Section 3.1, UDAQ developed a newer CB05 emission inventory based on the 2011 NEI. UDAQ further developed a set of alternative NOx and VOC scenarios to investigate CAMx sensitivity to emissions from the O&G sector. We have run CAMx v6.1 with the snow and CB6r3 updates for the February 2013 modeling episode using these new emissions. Evidence from our initial tests indicated that the model over predicts N_2O_5 at night by a factor of about 20. Therefore, this series of tests also included an additional CB6r3 update that increased the rate constant for heterogeneous N_2O_5 hydrolysis to nitric acid by a factor of 20 (see reaction 39 in Appendix A).

Five additional CAMx simulations were conducted in the order listed below:

- Base (CAMx v6.1, CB6r3, snow updates, 2011 NEI, increased heterogeneous N_2O_5 hydrolysis);
- NOx/3 (O&G inventory NOx divided by 3);
- NOx/3+VOC×2.5 (O&G inventory VOC multiplied by 2.5);
- NOx/3+VOCx2.5+Surface Model (Addition of surface chemistry for HONO);
- NOx/3+VOC×2.5+Formaldehyde (Additional formaldehyde added to O&G inventory)

In the fourth simulation, the CAMx surface model is configured to track peroxynitric acid (PNA) and HNO_3 deposition to the snowpack and to generate HONO via thermal reaction (from PNA) and photolysis (from HNO_3). The specific surface model parameters are shown in Figure 3-6. The rate of irreversible loss into the snowpack results in a lifetime of about 5 days for all three compounds. The PNA to HONO rate results in a PNA lifetime of approximately 10 minutes but this contribution is expected to be minor given the small amount of deposited PNA. The HNO_3 to HONO channel is expected to be the largest source of surface HONO given the large amount of deposited HNO_3. The HNO_3 to HONO rate is approximated to yield a mean atmospheric HONO concentration of about 0.1 ppb, with peak HONO not exceeding 0.5 ppb, consistent with HONO measured by Differential Optical Absorption Spectroscopy (DOAS) in 2012 and 2014 (Stoeckenius, 2015). We have confirmed that the surface model indeed results in HONO air concentrations of about 0.1 ppb. Without the surface model, HONO air concentrations are an order of magnitude lower.

In the fifth simulation, additional formaldehyde emissions are added to the O&G inventory in an attempt to match observations at Horesepool during the 2013 UBOS. The source of abundant formaldehyde remains uncertain, although there is evidence to suggest that primary and secondary sources of formaldehyde may be related to the widespread use of methanol as

```
Surface Model
Species          SoilSorb SoilLeach   VegSorb    VegPen   SnoSorb    SnoMlt
  1  HNO3        1.00E+10  1.00E-10  1.00E+10  1.00E-10  1.00E+10  9.70E-05
  2  PNA         1.00E+10  1.00E-10  1.00E+10  1.00E-10  1.00E+10  9.70E-05
  3  HONO        1.00E+00  1.00E-10  1.00E+00  1.00E-10  1.00E+00  9.70E-05
Rxn  Precursor Product       Soil K    Soil J     Veg K     Veg J    Snow K    Snow J
  1  HNO3       HONO        0.00E+00  0.00E+00  0.00E+00  0.00E+00  0.00E+00  1.00E-03
  2  PNA        HONO        0.00E+00  0.00E+00  0.00E+00  0.00E+00  1.00E-01  0.00E+00
```

Figure 3-6. CAMx surface model chemistry parameters used for sensitivity testing. In this case, 3 gases are treated, where PNA and HNO_3 deposited to the snowpack react to form HONO, which is released back to the atmosphere. Refer to Section 2.1.3.1 for a description of variables and units.

an anti-freeze agent. To simulate a widespread source, UDAQ increased formaldehyde emissions by a factor of 12.5 over the amount reported for the O&G sector in the 2011 NEI.

3.2.1 Sensitivity Results

Figure 3-7 displays time series of measured and simulated hourly ozone, NOx and several NOx oxidation products (collectively referred to as NOy), and several VOC compounds at Horsepool during the simulation period. Plots show results for each of the five simulations described above. The NOx reduction case is effective at reducing simulated NO to measured levels and the timing of peak NO agrees well (Figure 3-7(b)), but NO_2 continues to chemically build up each day and over predicts by factors of 4 or more (Figure 3-7(c)). NOx reductions also result in minor reductions in HNO_3 and N_2O_5, exacerbating under predictions of HNO_3 (Figure 3-7(d) while marginally improving large over predictions of N_2O_5 (Figure 3-7(e)). The combination of NOx reductions and VOC increases result in negligible increases in peroxyacetyl nitrate (PAN), which remains under predicted by factors of about 10 (Figure 3-7(f)). Even with a large reduction in NOx emissions, the model's surface layer remains NOx-rich and ozone production is NOx-inhibited.

Part of the NOy problem may be related to the fact that all O&G sector emissions developed for modeling are treated as area sources and injected into the surface layer (12 m deep) where they are confined during stable conditions. NOx is emitted by combustion sources that are buoyant, which may rise to more than 12 m and remain decoupled from the surface layer for extended periods. If NOx emissions are injected above the surface layer there would be vertical separation between VOC and NOx emissions, resulting in lower surface NOx concentrations than in the current model and better agreement with ambient data.

The VOC enhancement case is effective at increasing alkanes (Ethane, Figure 3-7(g)) and aromatics (toluene and xylene, Figures 3-7(i) and 3-7(j)) to near observed levels, but ethene is apparently missing from the emissions inventory (Figure 3-7(h)). Although alkanes are the dominant form of VOC from O&G emissions, they are low in reactivity. Furthermore, the timing of peak VOC concentrations tend not to agree well with measurements, indicating possible issues with emission temporal profiles or the timing of meteorological shifts (e.g., vertical

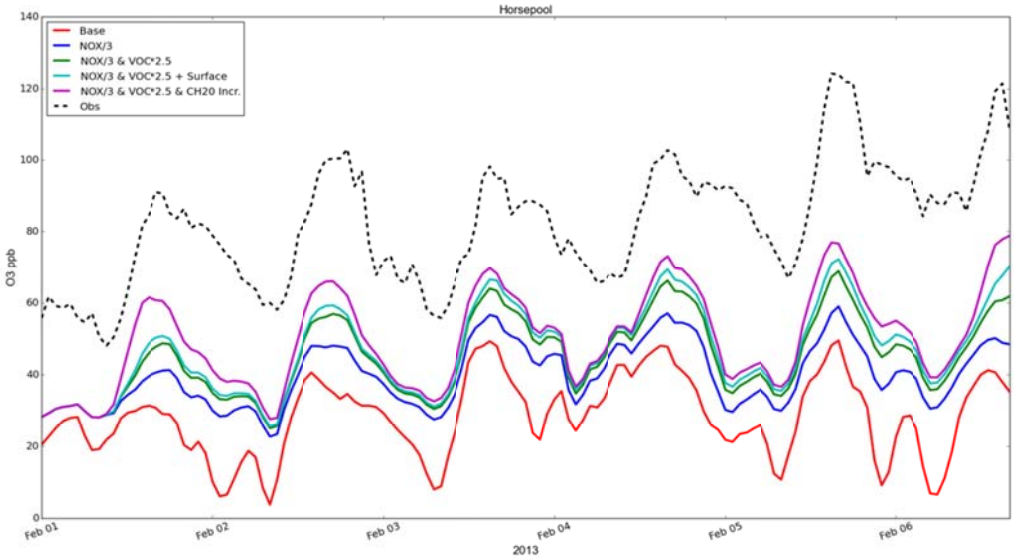

Figure 3-7(a). Ozone time series at Horsepool over February 1-6, 2013 showing measurements and results from five CAMx simulations.

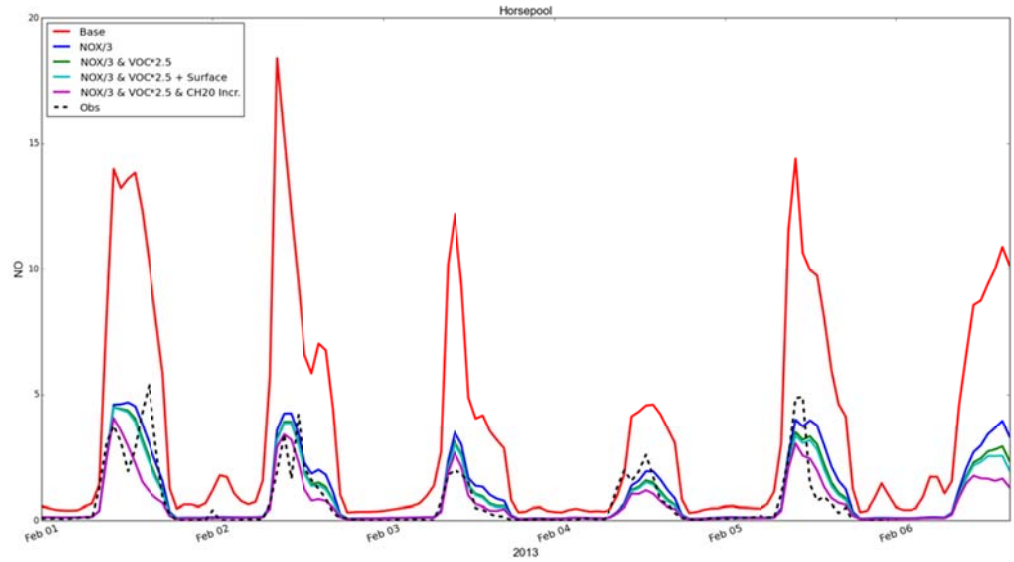

Figure 3-7(b). NO time series at Horsepool over February 1-6, 2013 showing measurements and results from five CAMx simulations.

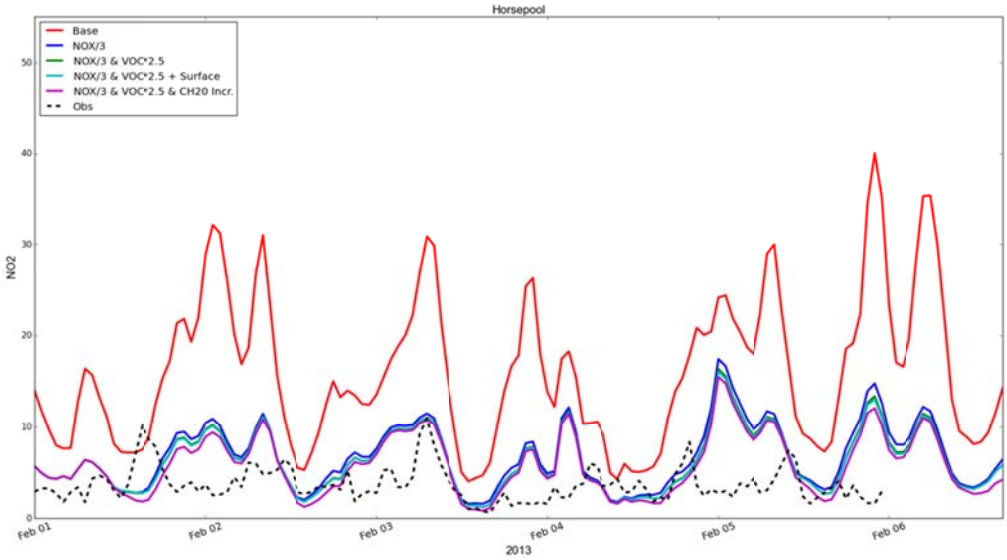

Figure 3-7(c). NO_2 time series at Horsepool over February 1-6, 2013 showing measurements and results from five CAMx simulations.

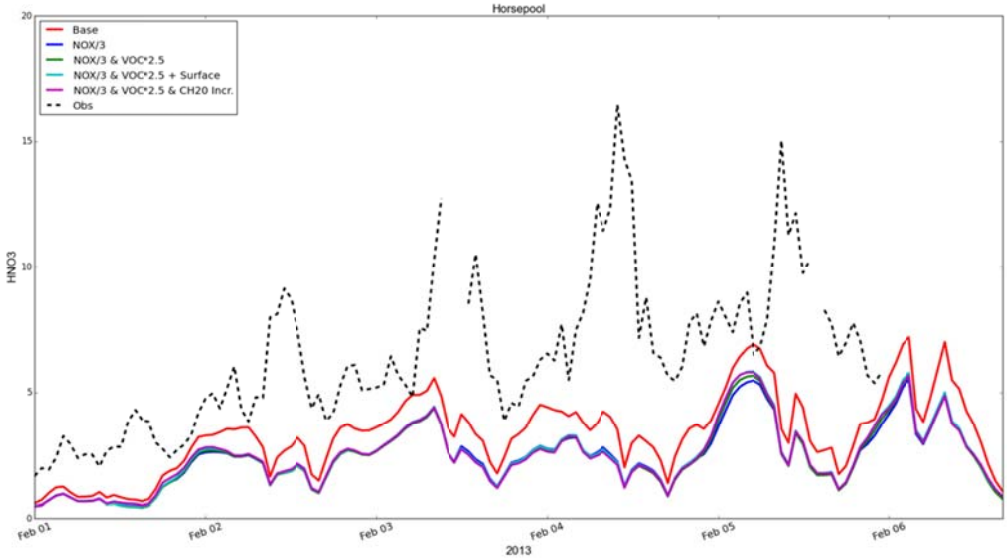

Figure 3-7(d). HNO_3 time series at Horsepool over February 1-6, 2013 showing measurements and results from five CAMx simulations.

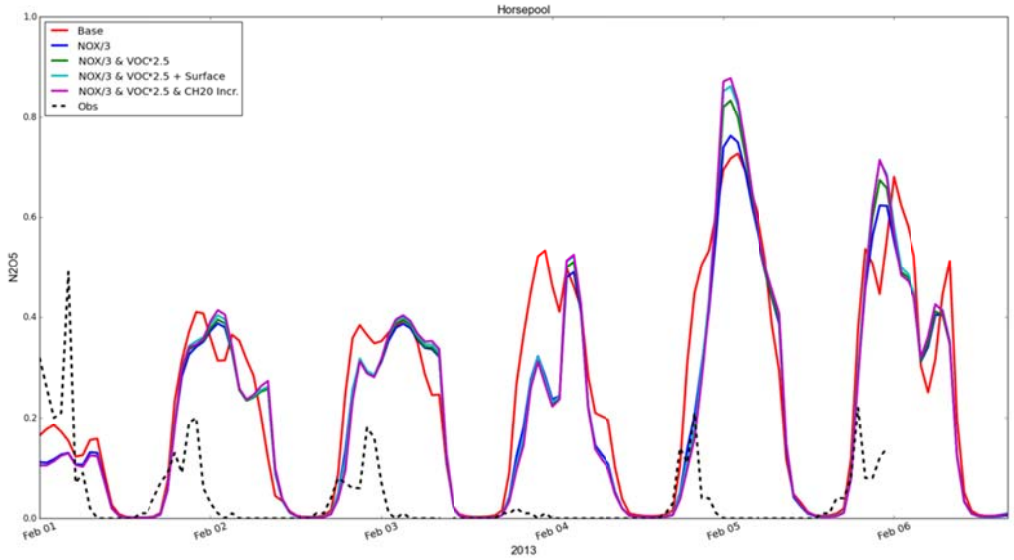

Figure 3-7(e). N_2O_5 time series at Horsepool over February 1-6, 2013 showing measurements and results from five CAMx simulations.

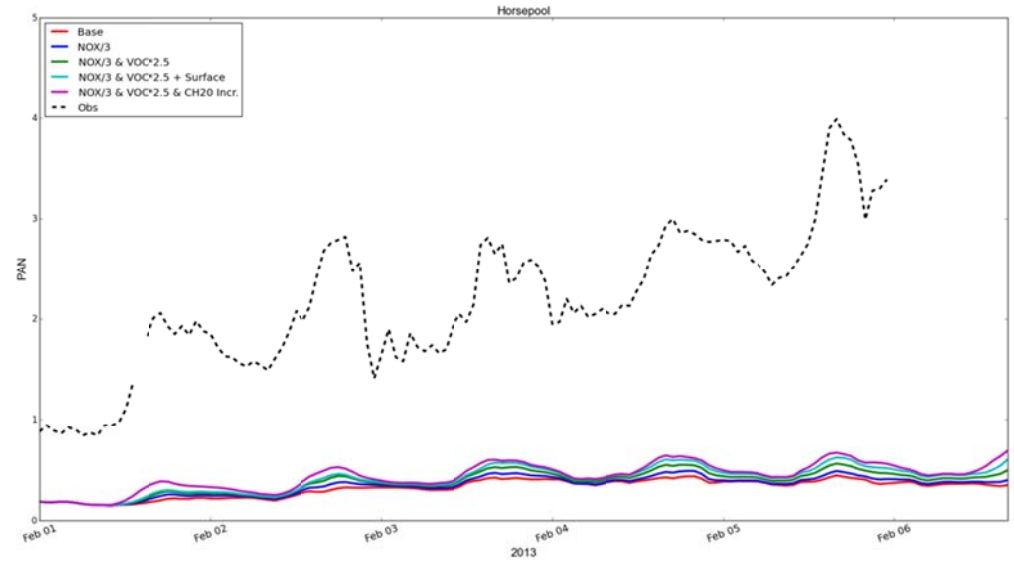

Figure 3-7(f). PAN time series at Horsepool over February 1-6, 2013 showing measurements and results from five CAMx simulations.

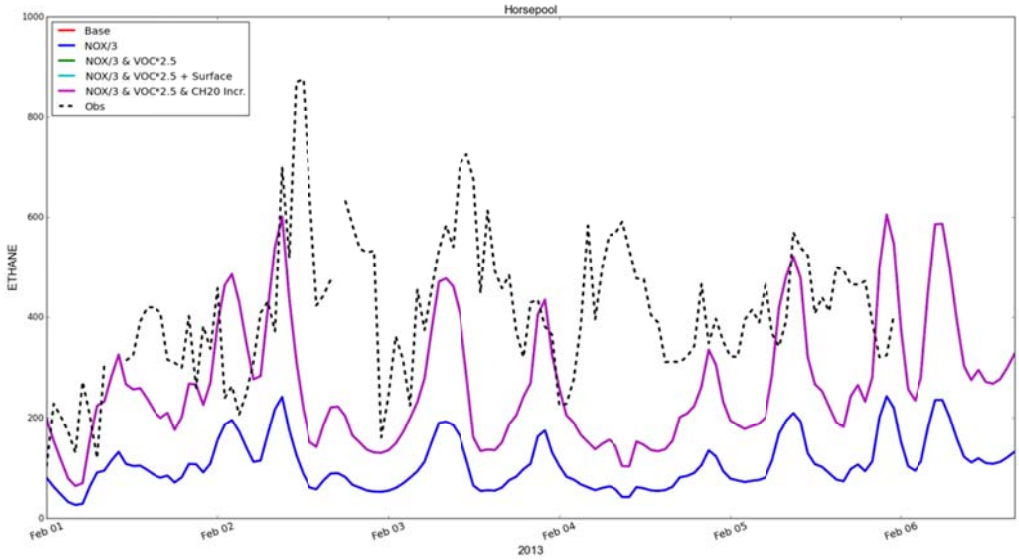

Figure 3-7(g). Ethane time series at Horsepool over February 1-6, 2013 showing measurements and results from five CAMx simulations.

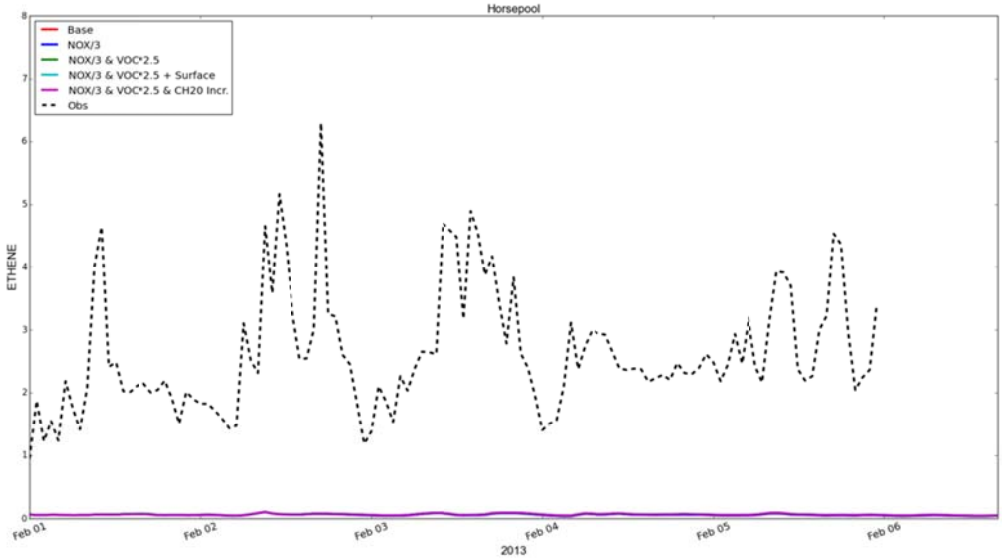

Figure 3-7(h). Ethene time series at Horsepool over February 1-6, 2013 showing measurements and results from five CAMx simulations.

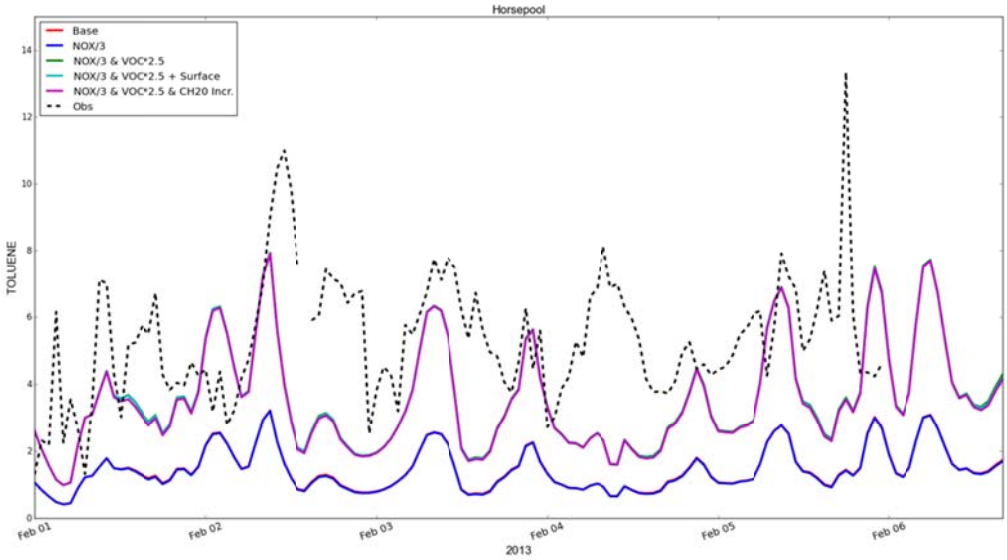

Figure 3-7(i). Toluene time series at Horsepool over February 1-6, 2013 showing measurements and results from five CAMx simulations.

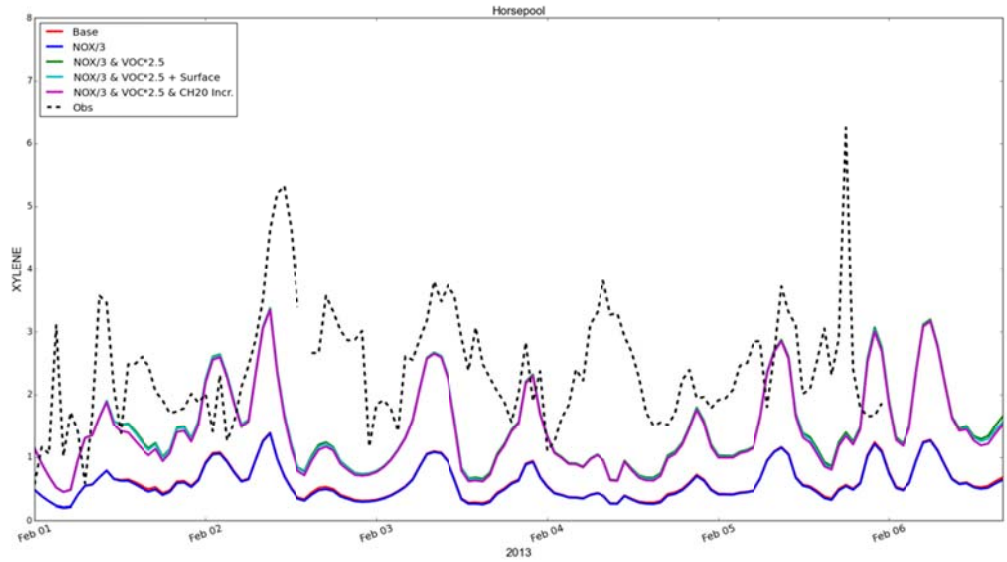

Figure 3-7(j). Xylene time series at Horsepool over February 1-6, 2013 showing measurements and results from five CAMx simulations.

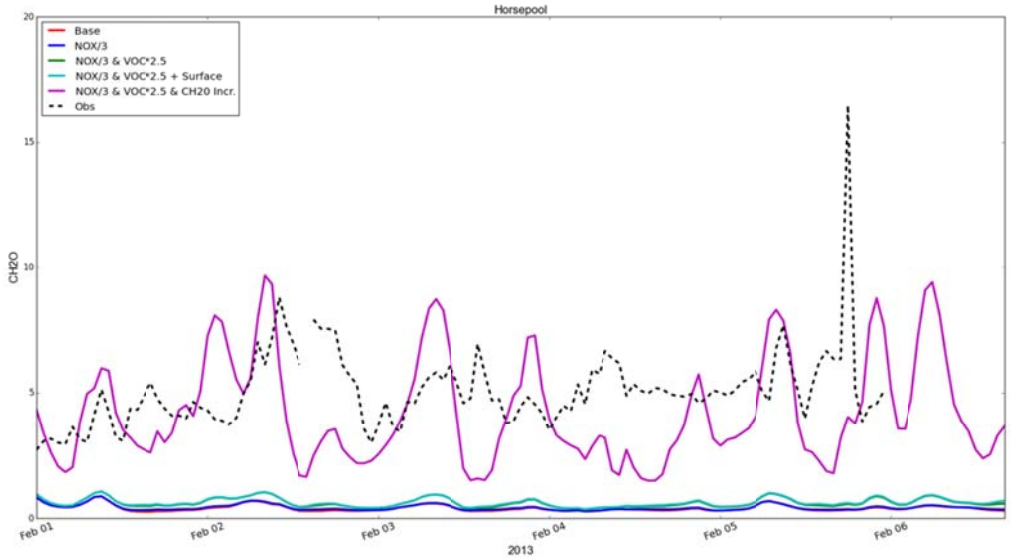

Figure 3-7(k). Formaldehyde time series at Horsepool over February 1-6, 2013 showing measurements and results from five CAMx simulations.

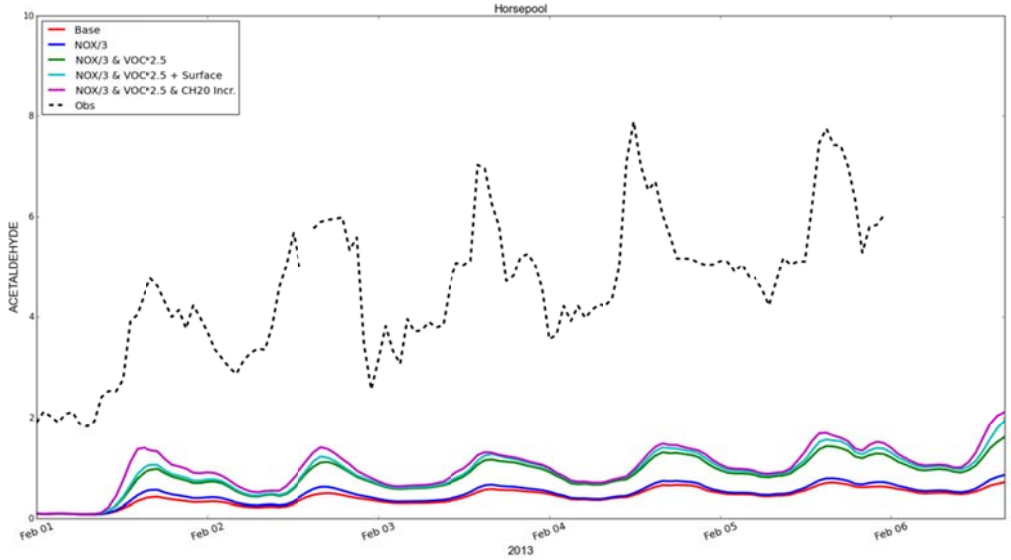

Figure 3-7(l). Acetaldehyde time series at Horsepool over February 1-6, 2013 showing measurements and results from five CAMx simulations.

mixing or transport patterns). A large fraction of VOC from the O&G sector occurs from fugitive sources (from valves, flanges and storage tanks). These types of emissions are highly variable and thus their strength, location and timing are difficult to characterize in emission inventories. Since they are non-buoyant, VOC emissions may remain vertically decoupled from buoyant NOx emissions for many hours.

Aldehydes are only marginally impacted by the VOC scale-up (Figures 3-7(k) and 3-7(l)), indicating that the base inventory is specifically lacking carbonyls. Formaldehyde agreement improves only when additional emissions of this compound are added to the inventory, yet again the timing of peak concentrations remains poor. A mechanism to increase acetaldehyde by a factor of about 5 is also needed, but was not tested.

Ozone time series at Horsepool (Figure 3-7(a)) indicate incremental improvements with each change to the emission inventory and the addition of HONO production in the surface model. However, peak ozone reaches about 80 ppb while observations exceed 120 ppb. Nearly equivalent ozone increases are achieved with NOx reductions, VOC increases, and the addition of formaldehyde. The addition of HONO surface chemistry produces HONO concentrations comparable to measurements made by DOAS (about 0.1 ppb), but increases ozone by a few ppb at most. Tests of the snow surface chemistry model confirm functionality, but cannot determine whether or not snow chemistry is important in the Uinta basin because more research is needed to specify model parameters.

Ozone is equivalently under predicted throughout the basin for all simulated cases, as shown in Figure 3-8. Despite all precursor changes applied in these tests, ozone response is limited and the relative mix of individual NOy and VOC compounds at Horsepool does not match observed conditions. This implies missing reactivity among ozone precursors, which cannot be explained by the use of CB05 emissions with the CB6 chemistry.

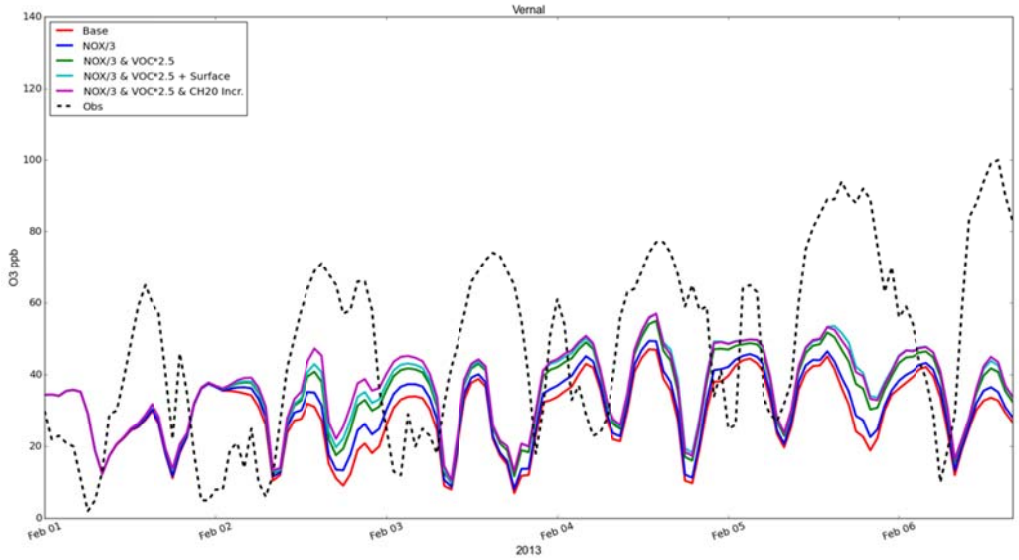

Figure 3-8(a). Ozone time series at Vernal over February 1-6, 2013 showing measurements and results from five CAMx simulations.

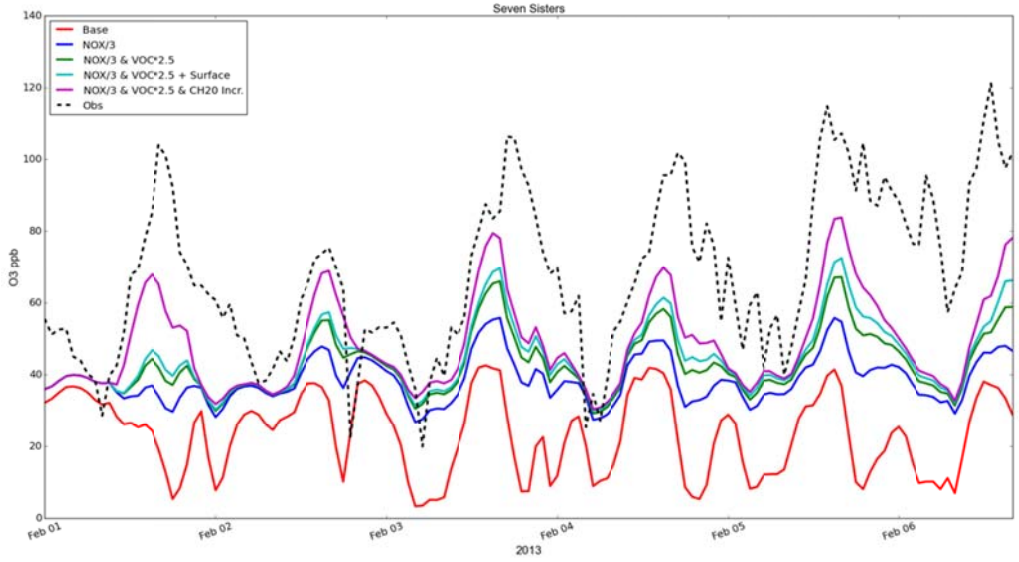

Figure 3-8(b). Ozone time series at Seven Sisters over February 1-6, 2013 showing measurements and results from five CAMx simulations.

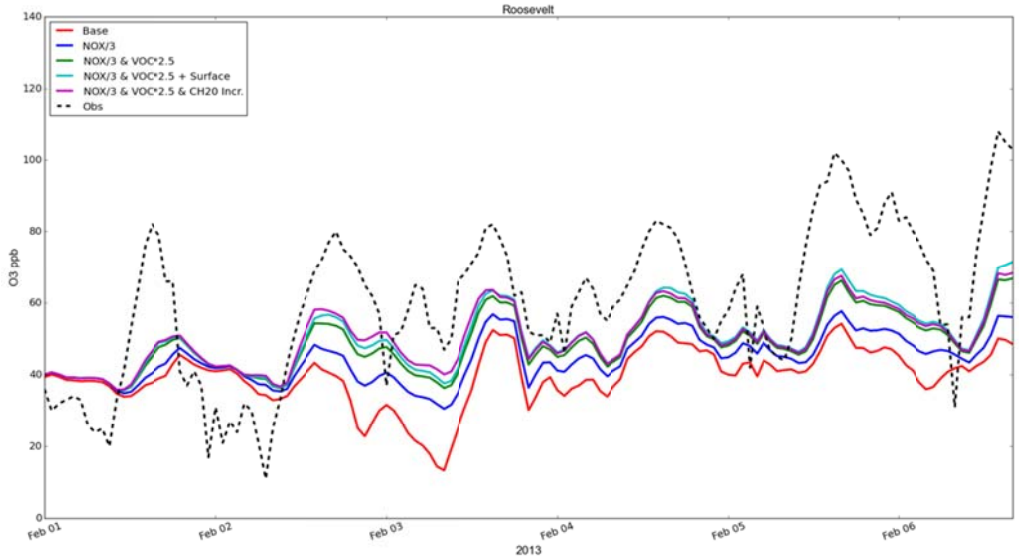

Figure 3-8(c). Ozone time series at Roosevelt over February 1-6, 2013 showing measurements and results from five CAMx simulations.

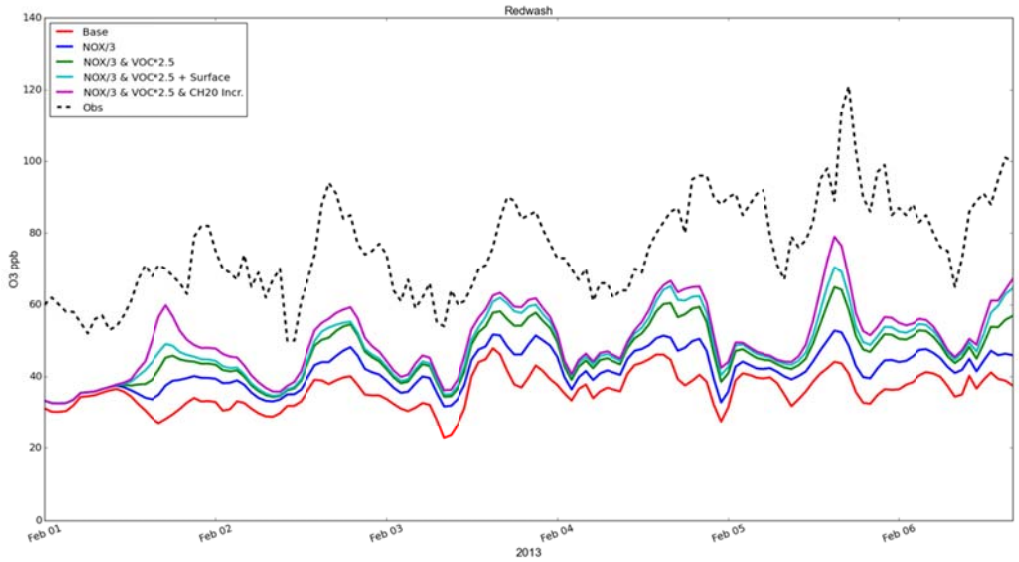

Figure 3-8(d). Ozone time series at Redwash over February 1-6, 2013 showing measurements and results from five CAMx simulations.

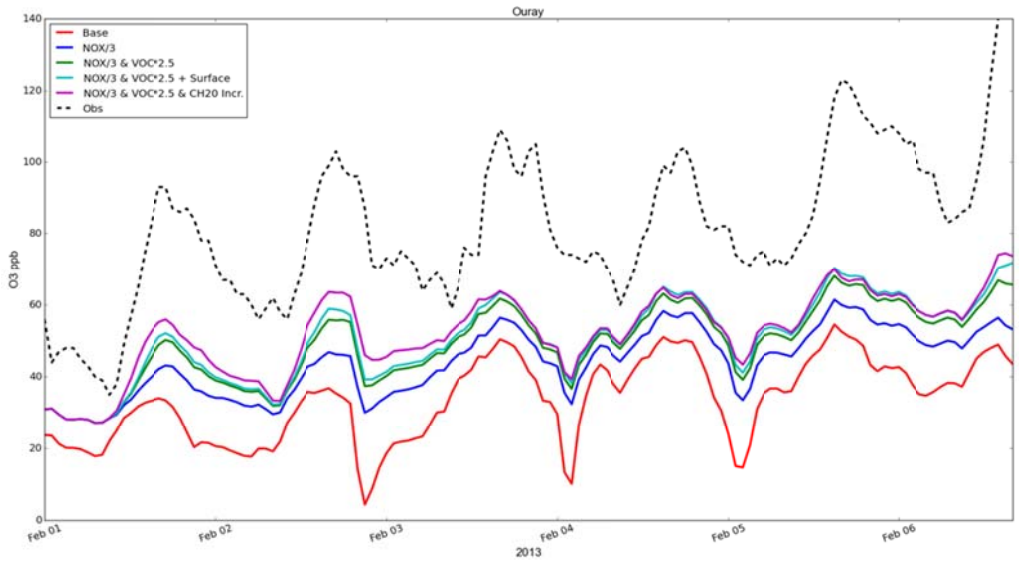

Figure 3-8(e). Ozone time series at Ouray over February 1-6, 2013 showing measurements and results from five CAMx simulations.

4.0 CONCLUSIONS AND RECOMMENDATIONS

Ramboll Environ has developed and evaluated specific updates to CAMx to improve the simulation of wintertime photochemistry. We improved the characterization of snow cover and its influence on atmospheric photolysis, dry deposition of gases and particles, and surface chemistry. We updated the Carbon Bond chemical mechanism (CB6r3) to account for the influence of temperature and pressure on the formation of organic nitrates from reactions of VOC and NOx. These chemistry updates were transferred to model developers at the EPA, who incorporated CB6r3 into CMAQ.

The CAMx updates were tested in simulations using model inputs provided by UDAQ. The updates improve ozone simulations for the Uinta Basin by producing changes that are in line with expectations with respect to direction and magnitude. The updates to air chemistry in CB6r3 lower NOx at cold temperatures, which reduces ozone production slightly (<5 ppb) in our tests. The updates to the snow treatment increase surface albedo, thereby increasing photolysis, and reducing deposition rates for ozone and precursors. Collectively these snow modifications increase ozone moderately (5-10 ppb) in our tests. Surface chemistry on or within the snowpack may be a source of photochemically reactive compounds such as HONO that promote ozone production. Recent literature reviews conclude that snow chemistry mechanisms are complex, uncertain, and inconclusive, with more research needed. Tests of the snow surface chemistry model confirm functionality, but cannot determine whether or not snow chemistry is important in the Uinta basin because more research is needed to specify model parameters. The CAMx snow surface chemistry model can be used to test and evaluate results from future field experiments in the Uinta basin.

The model updates described here are insufficient by themselves to simulate ozone at measured levels throughout the Uinta Basin. The model exhibits strong sensitivity when NOx and VOC emission estimates are adjusted to better align with measurements recorded during the 2013 UBOS. But, even after NOx and VOC emission adjustments, the relative proportions of NOx oxidation products and certain individual VOC species remain incorrectly replicated, indicating that the simulated emission-chemistry cycle is not correct. Therefore, additional work is needed to further improve the Uinta Basin emission inventory.

Stemming from analyses reported here, we recommend improvements in the following three areas:

- NOx is far too abundant: this may be the result of an improper treatment of the vertical distribution of NOx in the model. Future inventories should move NOx sources such as engines, pumps and compressors from the area source inventory to specific point sources with stack parameters from which to calculate plume rise.
- VOC is far too deficient: the consistent under-estimates among alkanes, alkenes and aromatics are indications of one or more misrepresented sources, such as insufficient fugitive emissions. The VOC mapping scheme should be updated from CB05 to CB6 to maximize the benefits gained from the updates in CB6r3 chemistry mechanism.

- Aldehydes are far too deficient: Specifically there is too little formaldehyde in the inventory, by factors that are far larger than other VOC (alkanes, aromatics). This suggests a missing a source.

5.0 REFERENCES

Ahmadov, R. S. McKeen, M. Trainer, R. Banta, A. Brewer, S. Brown, P.M. Edwards, J.A. de Gouw, G.J. Frost, J. Gilman, D. Helmig, B. Johnson, A. Karion, A. Koss, A. Langford, B. Lerner, J. Olson, S. Oltmans, J. Peischl, G. Pétron, Y. Pichugina, J.M. Roberts, T. Ryerson, R. Schnell, C. Senff, C. Sweeney, C. Thompson, P. Veres, C. Warneke, R. Wild, E. J. Williams, B. Yuan, R. Zamora, 2014. Understanding high wintertime ozone pollution events in an oil and natural gas producing region. *Atmos. Chem. Phys. Discuss.*, 14, 20295–20343, doi:10.5194/acpd-14-20295-2014.

Arey, J., S.M. Aschmann, E.S.C. Kwok, R. Atkinson, 2001. Alkyl nitrate, hydroxyalkyl nitrate, and hydroxycarbonyl formation from the NO x-air photooxidations of C5-C8 n-alkanes. *Journal of Physical Chemistry*, A 105, 1020-1027.

Atkinson, R., W.P. Carter, A.M. Winer, 1983. Effects of temperature and pressure on alkyl nitrate yields in the nitrogen oxide (NOx) photooxidations of n-pentane and n-heptane. *Journal of Physical Chemistry*, 87(11), 2012-2018.

Atkinson, R., D.L. Baulch, R.A. Cox, J.N. Crowley, R.F. Hampson, R.G. Hynes, M.E. Jenkin, M.J. Rossi, J. Troe, 2004. Evaluated kinetic and photochemical data for atmospheric chemistry: Volume I-gas phase reactions of O x, HO x, NO x and SO x species. *Atmospheric chemistry and physics*, 4, 1461-1738.

Barlage, M., F. Chen, M. Tewari, K. Ikeda, D. Gochis, J. Dudhia, R. Rasmussen, B. Livneh, M. Ek, K. Mitchell, 2010. Noah land surface model modifications to improve snowpack prediction in the Colorado Rocky Mountains, *J. Geophys. Res.*, 115, D22101, doi:10.1029/2009JD013470.

Byun, D.W., and K.L. Schere, 2006. Review of the governing equations, computational algorithms, and other components of the Models-3 Community Multiscale Air Quality (CMAQ) Modeling System. *Appl. Mech. Rev.*, 59, 51-77.

Carter, W.P.L. and J.H. Seinfeld, 2012. Winter ozone formation and VOC incremental reactivities in the Upper Green River Basin of Wyoming. *Atmospheric Environment*, 50, 255-266.

Carter, W.P. and G. Heo, 2013. Development of revised SAPRC aromatics mechanisms. *Atmospheric Environment*, 77, 404-414.

Chen, F., and J. Dudhia, 2001. Coupling an advanced land surface–hydrology model with the Penn State–NCAR MM5 modeling system, Part I: Model implementation and sensitivity. *Mon. Wea. Rev.*, 129, 569–585.

Ek, M.B., K.E. Mitchell, Y. Lin, E. Rogers, P. Grunmann, V. Koren, G. Gayno, J. D. Tarpley, 2003. Implementation of Noah land surface model advances in the National Centers for Environmental Prediction operational mesoscale Eta model. *J. Geophys. Res.*, 108(D22), 8851, doi:10.1029/2002JD003296.

ENVIRON, 2014. User's Guide: Comprehensive Air quality Model with extensions (CAMx), Version 6.10. ENVIRON International Corporation, Novato, CA (www.camx.com).

Herman, J., and E. Celarier, 1997. Earth surface reflectivity climatology at 340-380 nm from TOMS data. *J. Geophys. Res.*, 102, 23.

Hildebrandt Ruiz, L. and G. Yarwood, 2013. Interactions between Organic Aerosol and NOy: Influence on Oxidant Production. Final report for AQRP project 12-012. Available at http://aqrp.ceer.utexas.edu/projectinfoFY12_13%5C12-012%5C12-012%20Final%20Report.pdf.

Goliff, W.S., W.R. Stockwell, C.V. Lawson, 2013. The regional atmospheric chemistry mechanism, version 2. *Atmospheric Environment*, 68, 174-185.

Lee, L., P.J. Wooldridge, J.B. Gilman, C. Warneke, J. de Gouw, R.C. Cohen, 2014. Low temperatures enhance organic nitrate formation: evidence from observations in the 2012 Uintah Basin Winter Ozone Study. *Atmospheric Chemistry and Physics Discussions*, 14(11), 17401-17438.

Lefer, B., J. Stutz, W. Vizuete, E. Couzo, G. Yarwood, P. Karamchandani, 2014. Implementation and evaluation of new HONO Mechanisms in a 3-D chemical transport model for spring 2009 in Houston. Final Report for AQRP Project 12-028. Prepared for the Texas Air Quality Research Program (http://aqrp.ceer.utexas.edu/projectinfoFY12_13/12-028/12-028%20Final%20Report.pdf).

Livneh, B., Y. Xia, K. E. Mitchell, M. B. Ek, 2010. Noah LSM snow model diagnostics and enhancements. *J. Hydromet.*, 11, doi:10.1175/2009JHM1174.1.

NCAR, 2011. The Tropospheric Visible and Ultraviolet (TUV) Radiation Model web page. National Center for Atmospheric Research, Atmospheric Chemistry Division, Boulder, Colorado (http://cprm.acd.ucar.edu/Models/TUV/index.shtml).

Perring, A.E., S.E. Pusede, R.C. Cohen, 2013. An observational perspective on the atmospheric impacts of alkyl and multifunctional nitrates on ozone and secondary organic aerosol. *Chemical reviews*, 113(8), 5848-5870.

Robinson, D., and G. Kulka, 1985. Maximum surface albedo of seasonally snow-covered lands in the northern hemisphere. *J. Clim. Appl. Met.*, 24, 402-411.

Stoeckenius, T. (Ed.), 2015. Final Report: 2014 Uinta Basin Winter Ozone Study. Prepared for the Utah Division of Air Quality, Salt Lake City, UT (February 2015) http://www.deq.utah.gov/locations/U/uintahbasin/ozone/docs/2015/02Feb/UBWOS_2014_Final.pdf.

U.S. Army Corps Of Engineers, 1956. Snow hydrology: Summary report of the snow investigations. U. S. Army of Engineers North Pacific Division, 437 pp.

Wang, Z., and X. Zeng, 2010. Evaluation of snow albedo in land models for weather and climate studies. *J. Appl. Met Clim.*, 49, doi: 10.1175/2009JAMC2134.1.

Wesely, M., 1989. Parameterization of surface resistances to gaseous dry deposition in regional-scale models. *Atmos. Environ.*, 23, 1293-1304.

Whitten, G.Z., G. Heo, Y. Kimura, E. McDonald-Buller, D.T. Allen, W.P. Carter, G. Yarwood, 2010. A new condensed toluene mechanism for Carbon Bond: CB05-TU. *Atmospheric Environment*, 44(40), 5346-5355.

Wiscombe, W.J., and S.G. Warren, 1980. A model for the spectral albedo of snow, I: Pure snow. *J. Atmos. Sci.*, 37, 2712–2733.

Yeh, G.K. and P.J. Ziemann, 2014. Alkyl Nitrate Formation from the Reactions of C8–C14 n-Alkanes with OH Radicals in the Presence of NO x: Measured Yields with Essential Corrections for Gas–Wall Partitioning. *The Journal of Physical Chemistry A,* 118 (38), 8797-8806.

Zhang, L., J. Brook, R. Vet, 2003. A revised parameterization for gaseous dry deposition in air quality models. A*tmos. Chem. Phys.*, 3, 2067-2082.

RAMBOLL ENVIRON

APPENDIX A
Listing of the CB6r3 Chemical Mechanism

Appendix A. Listing of the CB6r3 Chemical Mechanism

Number	Reactants and Products	Rate Constant Expression	k_{298}
1	NO2 = NO + O	Photolysis	6.30E-3
2	O + O2 + M = O3 + M	k = 5.68E-34 (T/300)^-2.6	5.78E-34
3	O3 + NO = NO2	k = 1.40E-12 exp(-1310/T)	1.73E-14
4	O + NO + M = NO2 + M	k = 1.00E-31 (T/300)^-1.6	1.01E-31
5	O + NO2 = NO	k = 5.50E-12 exp(188/T)	1.03E-11
6	O + NO2 = NO3	Falloff: F=0.6; n=1 k(0) = 1.30E-31 (T/300)^-1.5 k(inf) = 2.30E-11 (T/300)^0.24	2.11E-12
7	O + O3 =	k = 8.00E-12 exp(-2060/T)	7.96E-15
8	O3 = O	Photolysis	3.33E-4
9	O3 = O1D	Photolysis	8.78E-6
10	O1D + M = O + M	k = 2.23E-11 exp(115/T)	3.28E-11
11	O1D + H2O = 2 OH	k = 2.14E-10	2.14E-10
12	O3 + OH = HO2	k = 1.70E-12 exp(-940/T)	7.25E-14
13	O3 + HO2 = OH	k = 2.03E-16 (T/300)^4.57 exp(693/T)	2.01E-15
14	OH + O = HO2	k = 2.40E-11 exp(110/T)	3.47E-11
15	HO2 + O = OH	k = 2.70E-11 exp(224/T)	5.73E-11
16	OH + OH = O	k = 6.20E-14 (T/298)^2.6 exp(945/T)	1.48E-12
17	OH + OH = H2O2	Falloff: F=0.5; n=1.13 k(0) = 6.90E-31 (T/300)^-0.8 k(inf) = 2.60E-11	5.25E-12
18	OH + HO2 =	k = 4.80E-11 exp(250/T)	1.11E-10
19	HO2 + HO2 = H2O2	k = k1 + k2 [M] k1 = 2.20E-13 exp(600/T) k2 = 1.90E-33 exp(980/T)	2.90E-12
20	HO2 + HO2 + H2O = H2O2	k = k1 + k2 [M] k1 = 3.08E-34 exp(2800/T) k2 = 2.66E-54 exp(3180/T)	6.53E-30
21	H2O2 = 2 OH	Photolysis	3.78E-6
22	H2O2 + OH = HO2	k = 2.90E-12 exp(-160/T)	1.70E-12
23	H2O2 + O = OH + HO2	k = 1.40E-12 exp(-2000/T)	1.70E-15
24	NO + NO + O2 = 2 NO2	k = 3.30E-39 exp(530/T)	1.95E-38
25	HO2 + NO = OH + NO2	k = 3.45E-12 exp(270/T)	8.54E-12
26	NO2 + O3 = NO3	k = 1.40E-13 exp(-2470/T)	3.52E-17
27	NO3 = NO2 + O	Photolysis	1.56E-1
28	NO3 = NO	Photolysis	1.98E-2
29	NO3 + NO = 2 NO2	k = 1.80E-11 exp(110/T)	2.60E-11
30	NO3 + NO2 = NO + NO2	k = 4.50E-14 exp(-1260/T)	6.56E-16
31	NO3 + O = NO2	k = 1.70E-11	1.70E-11
32	NO3 + OH = HO2 + NO2	k = 2.00E-11	2.00E-11
33	NO3 + HO2 = OH + NO2	k = 4.00E-12	4.00E-12
34	NO3 + O3 = NO2	k = 1.00E-17	1.00E-17
35	NO3 + NO3 = 2 NO2	k = 8.50E-13 exp(-2450/T)	2.28E-16
36	NO3 + NO2 = N2O5	Falloff: F=0.35; n=1.33 k(0) = 3.60E-30 (T/300)^-4.1 k(inf) = 1.90E-12 (T/300)^0.2	1.24E-12
37	N2O5 = NO3 + NO2	Falloff: F=0.35; n=1.33	4.46E-2

		k(0) = 1.30E-3 (T/300)^-3.5 exp(-11000/T) k(inf) = 9.70E+14 (T/300)^0.1 exp(-11080/T)	
38	N2O5 = NO2 + NO3	Photolysis	2.52E-5
39	N2O5 + H2O = 2 HNO3	k = 1.00E-22	1.00E-22
40	NO + OH = HONO	Falloff: F=0.81; n=0.87 k(0) = 7.40E-31 (T/300)^-2.4 k(inf) = 3.30E-11 (T/300)^-0.3	9.77E-12
41	NO + NO2 + H2O = 2 HONO	k = 5.00E-40	5.00E-40
42	HONO + HONO = NO + NO2	k = 1.00E-20	1.00E-20
43	HONO = NO + OH	Photolysis	1.04E-3
44	HONO + OH = NO2	k = 2.50E-12 exp(260/T)	5.98E-12
45	NO2 + OH = HNO3	Falloff: F=0.6; n=1 k(0) = 1.80E-30 (T/300)^-3 k(inf) = 2.80E-11	1.06E-11
46	HNO3 + OH = NO3	k = k1 + k3 [M] / (1 + k3 [M] / k2) k1 = 2.40E-14 exp(460/T) k2 = 2.70E-17 exp(2199/T) k3 = 6.50E-34 exp(1335/T)	1.54E-13
47	HNO3 = OH + NO2	Photolysis	2.54E-7
48	HO2 + NO2 = PNA	Falloff: F=0.6; n=1 k(0) = 1.80E-31 (T/300)^-3.2 k(inf) = 4.70E-12	1.38E-12
49	PNA = HO2 + NO2	Falloff: F=0.6; n=1 k(0) = 4.10E-5 exp(-10650/T) k(inf) = 4.80E+15 exp(-11170/T)	8.31E-2
50	PNA = 0.59 HO2 + 0.59 NO2 + 0.41 OH + 0.41 NO3	Photolysis	2.36E-6
51	PNA + OH = NO2	k = 3.20E-13 exp(690/T)	3.24E-12
52	SO2 + OH = SULF + HO2	Falloff: F=0.53; n=1.1 k(0) = 4.50E-31 (T/300)^-3.9 k(inf) = 1.30E-12 (T/300)^-0.7	8.12E-13
53	C2O3 + NO = NO2 + MEO2 + RO2	k = 7.50E-12 exp(290/T)	1.98E-11
54	C2O3 + NO2 = PAN	Falloff: F=0.3; n=1.41 k(0) = 2.70E-28 (T/300)^-7.1 k(inf) = 1.20E-11 (T/300)^-0.9	9.40E-12
55	PAN = NO2 + C2O3	Falloff: F=0.3; n=1.41 k(0) = 4.90E-3 exp(-12100/T) k(inf) = 5.40E+16 exp(-13830/T)	2.98E-4
56	PAN = 0.6 NO2 + 0.6 C2O3 + 0.4 NO3 + 0.4 MEO2 + 0.4 RO2	Photolysis	3.47E-7
57	C2O3 + HO2 = 0.41 PACD + 0.15 AACD + 0.15 O3 + 0.44 MEO2 + 0.44 RO2 + 0.44 OH	k = 5.20E-13 exp(980/T)	1.39E-11
58	C2O3 + RO2 = C2O3	k = 8.90E-13 exp(800/T)	1.30E-11
59	C2O3 + C2O3 = 2 MEO2 + 2 RO2	k = 2.90E-12 exp(500/T)	1.55E-11
60	C2O3 + CXO3 = MEO2 + ALD2 + XO2H + 2 RO2	k = 2.90E-12 exp(500/T)	1.55E-11
61	CXO3 + NO = NO2 + ALD2 + XO2H + RO2	k = 6.70E-12 exp(340/T)	2.10E-11
62	CXO3 + NO2 = PANX	k = k(ref) K k(ref) = k(54)	9.40E-12

		K = 1.00E+0	
63	PANX = NO2 + CXO3	k = k(ref) K k(ref) = k(55) K = 1.00E+0	2.98E-4
64	PANX = 0.6 NO2 + 0.6 CXO3 + 0.4 NO3 + 0.4 ALD2 + 0.4 XO2H + 0.4 RO2	Photolysis	3.47E-7
65	CXO3 + HO2 = 0.41 PACD + 0.15 AACD + 0.15 O3 + 0.44 ALD2 + 0.44 XO2H + 0.44 RO2 + 0.44 OH	k = 5.20E-13 exp(980/T)	1.39E-11
66	CXO3 + RO2 = 0.8 ALD2 + 0.8 XO2H + 0.8 RO2	k = 8.90E-13 exp(800/T)	1.30E-11
67	CXO3 + CXO3 = 2 ALD2 + 2 XO2H + 2 RO2	k = 3.20E-12 exp(500/T)	1.71E-11
68	RO2 + NO = NO	k = 2.40E-12 exp(360/T)	8.03E-12
69	RO2 + HO2 = HO2	k = 4.80E-13 exp(800/T)	7.03E-12
70	RO2 + RO2 =	k = 6.50E-14 exp(500/T)	3.48E-13
71	MEO2 + NO = FORM + HO2 + NO2	k = 2.30E-12 exp(360/T)	7.70E-12
72	MEO2 + HO2 = 0.9 MEPX + 0.1 FORM	k = 3.80E-13 exp(780/T)	5.21E-12
73	MEO2 + C2O3 = FORM + 0.9 HO2 + 0.9 MEO2 + 0.1 AACD + 0.9 RO2	k = 2.00E-12 exp(500/T)	1.07E-11
74	MEO2 + RO2 = 0.685 FORM + 0.315 MEOH + 0.37 HO2 + RO2	k = k(ref) K k(ref) = k(70) K = 1.00E+0	3.48E-13
75	XO2H + NO = NO2 + HO2	k = 2.70E-12 exp(360/T)	9.04E-12
76	XO2H + HO2 = ROOH	k = 6.80E-13 exp(800/T)	9.96E-12
77	XO2H + C2O3 = 0.8 HO2 + 0.8 MEO2 + 0.2 AACD + 0.8 RO2	k = k(ref) K k(ref) = k(58) K = 1.00E+0	1.30E-11
78	XO2H + RO2 = 0.6 HO2 + RO2	k = k(ref) K k(ref) = k(70) K = 1.00E+0	3.48E-13
79	XO2 + NO = NO2	k = k(ref) K k(ref) = k(75) K = 1.00E+0	9.04E-12
80	XO2 + HO2 = ROOH	k = k(ref) K k(ref) = k(76) K = 1.00E+0	9.96E-12
81	XO2 + C2O3 = 0.8 MEO2 + 0.2 AACD + 0.8 RO2	k = k(ref) K k(ref) = k(58) K = 1.00E+0	1.30E-11
82	XO2 + RO2 = RO2	k = k(ref) K k(ref) = k(70) K = 1.00E+0	3.48E-13
83	XO2N + NO = 0.5 NTR1 + 0.5 NTR2	k = k(ref) K k(ref) = k(75) K = 1.00E+0	9.04E-12
84	XO2N + HO2 = ROOH	k = k(ref) K k(ref) = k(76) K = 1.00E+0	9.96E-12
85	XO2N + C2O3 = 0.8 HO2 + 0.8 MEO2 + 0.2 AACD + 0.8 RO2	k = k(ref) K k(ref) = k(58) K = 1.00E+0	1.30E-11

86	XO2N + RO2 = RO2	k = k(ref) K k(ref) = k(70) K = 1.00E+0	3.48E-13
87	MEPX + OH = 0.6 MEO2 + 0.6 RO2 + 0.4 FORM + 0.4 OH	k = 5.30E-12 exp(190/T)	1.00E-11
88	MEPX = MEO2 + RO2 + OH	Photolysis	2.68E-6
89	ROOH + OH = 0.54 XO2H + 0.06 XO2N + 0.6 RO2 + 0.4 OH	k = 5.30E-12 exp(190/T)	1.00E-11
90	ROOH = HO2 + OH	Photolysis	2.68E-6
91	NTR1 + OH = NTR2	k = 2.00E-12	2.00E-12
92	NTR1 = NO2	Photolysis	1.06E-6
93	FACD + OH = HO2	k = 4.50E-13	4.50E-13
94	AACD + OH = MEO2 + RO2	k = 4.00E-14 exp(850/T)	6.93E-13
95	PACD + OH = C2O3	k = 5.30E-12 exp(190/T)	1.00E-11
96	FORM + OH = HO2 + CO	k = 5.40E-12 exp(135/T)	8.49E-12
97	FORM = 2 HO2 + CO	Photolysis	1.78E-5
98	FORM = CO + H2	Photolysis	2.38E-5
99	FORM + O = OH + HO2 + CO	k = 3.40E-11 exp(-1600/T)	1.58E-13
100	FORM + NO3 = HNO3 + HO2 + CO	k = 5.50E-16	5.50E-16
101	FORM + HO2 = HCO3	k = 9.70E-15 exp(625/T)	7.90E-14
102	HCO3 = FORM + HO2	k = 2.40E+12 exp(-7000/T)	1.51E+2
103	HCO3 + NO = FACD + NO2 + HO2	k = 5.60E-12	5.60E-12
104	HCO3 + HO2 = 0.5 MEPX + 0.5 FACD + 0.2 OH + 0.2 HO2	k = 5.60E-15 exp(2300/T)	1.26E-11
105	ALD2 + O = C2O3 + OH	k = 1.80E-11 exp(-1100/T)	4.49E-13
106	ALD2 + OH = C2O3	k = 4.70E-12 exp(345/T)	1.50E-11
107	ALD2 + NO3 = C2O3 + HNO3	k = 1.40E-12 exp(-1860/T)	2.73E-15
108	ALD2 = MEO2 + RO2 + CO + HO2	Photolysis	1.76E-6
109	ALDX + O = CXO3 + OH	k = 1.30E-11 exp(-870/T)	7.02E-13
110	ALDX + OH = CXO3	k = 4.90E-12 exp(405/T)	1.91E-11
111	ALDX + NO3 = CXO3 + HNO3	k = 6.30E-15	6.30E-15
112	ALDX = ALD2 + XO2H + RO2 + CO + HO2	Photolysis	6.96E-6
113	GLYD + OH = 0.2 GLY + 0.2 HO2 + 0.8 C2O3	k = 8.00E-12	8.00E-12
114	GLYD = 0.74 FORM + 0.89 CO + 1.4 HO2 + 0.15 MEOH + 0.19 OH + 0.11 GLY + 0.11 XO2H + 0.11 RO2	Photolysis	1.56E-6
115	GLYD + NO3 = HNO3 + C2O3	k = 1.40E-12 exp(-1860/T)	2.73E-15
116	GLY + OH = 1.8 CO + 0.2 XO2 + 0.2 RO2 + HO2	k = 3.10E-12 exp(340/T)	9.70E-12
117	GLY = 2 HO2 + 2 CO	Photolysis	5.50E-5
118	GLY + NO3 = HNO3 + 1.5 CO + 0.5 XO2 + 0.5 RO2 + HO2	k = 1.40E-12 exp(-1860/T)	2.73E-15
119	MGLY = C2O3 + HO2 + CO	Photolysis	1.46E-4
120	MGLY + NO3 = HNO3 + C2O3 + XO2 + RO2	k = 1.40E-12 exp(-1860/T)	2.73E-15
121	MGLY + OH = C2O3 + CO	k = 1.90E-12 exp(575/T)	1.31E-11
122	H2 + OH = HO2	k = 7.70E-12 exp(-2100/T)	6.70E-15
123	CO + OH = HO2	k = k1 + k2 [M] k1 = 1.44E-13 k2 = 3.43E-33	2.28E-13
124	CH4 + OH = MEO2 + RO2	k = 1.85E-12 exp(-1690/T)	6.37E-15

125	ETHA + OH = 0.991 ALD2 + 0.991 XO2H + 0.009 XO2N + RO2	k = 6.90E-12 exp(-1000/T)	2.41E-13
126	MEOH + OH = FORM + HO2	k = 2.85E-12 exp(-345/T)	8.95E-13
127	ETOH + OH = 0.95 ALD2 + 0.9 HO2 + 0.1 XO2H + 0.1 RO2 + 0.078 FORM + 0.011 GLYD	k = 3.00E-12 exp(20/T)	3.21E-12
128	KET = 0.5 ALD2 + 0.5 C2O3 + 0.5 XO2H + 0.5 CXO3 + 0.5 MEO2 + RO2 - 2.5 PAR	Photolysis	2.27E-7
129	ACET = 0.38 CO + 1.38 MEO2 + 1.38 RO2 + 0.62 C2O3	Photolysis	2.08E-7
130	ACET + OH = FORM + C2O3 + XO2 + RO2	k = 1.41E-12 exp(-620.6/T)	1.76E-13
131	PRPA + OH = XPRP	k = 7.60E-12 exp(-585/T)	1.07E-12
132	PAR + OH = XPAR	k = 8.10E-13	8.10E-13
133	ROR = 0.2 KET + 0.42 ACET + 0.74 ALD2 + 0.37 ALDX + 0.04 XO2N + 0.94 XO2H + 0.98 RO2 + 0.02 ROR - 2.7 PAR	k = 5.70E+12 exp(-5780/T)	2.15E+4
134	ROR + O2 = KET + HO2	k = 1.50E-14 exp(-200/T)	7.67E-15
135	ROR + NO2 = NTR1	k = 8.60E-12 exp(400/T)	3.29E-11
136	ETHY + OH = 0.7 GLY + 0.7 OH + 0.3 FACD + 0.3 CO + 0.3 HO2	Falloff: F=0.37; n=1.3 k(0) = 5.00E-30 (T/300)^-1.5 k(inf) = 1.00E-12	7.52E-13
137	ETH + O = FORM + HO2 + CO + 0.7 XO2H + 0.7 RO2 + 0.3 OH	k = 1.04E-11 exp(-792/T)	7.29E-13
138	ETH + OH = XO2H + RO2 + 1.56 FORM + 0.22 GLYD	Falloff: F=0.48; n=1.15 k(0) = 8.60E-29 (T/300)^-3.1 k(inf) = 9.00E-12 (T/300)^-0.85	7.84E-12
139	ETH + O3 = FORM + 0.51 CO + 0.16 HO2 + 0.16 OH + 0.37 FACD	k = 9.10E-15 exp(-2580/T)	1.58E-18
140	ETH + NO3 = 0.5 NO2 + 0.5 NTR1 + 0.5 XO2H + 0.5 XO2 + RO2 + 1.125 FORM	k = 3.30E-12 exp(-2880/T)	2.10E-16
141	OLE + O = 0.2 ALD2 + 0.3 ALDX + 0.1 HO2 + 0.2 XO2H + 0.2 CO + 0.2 FORM + 0.01 XO2N + 0.21 RO2 + 0.2 PAR + 0.1 OH	k = 1.00E-11 exp(-280/T)	3.91E-12
142	OLE + OH = 0.781 FORM + 0.488 ALD2 + 0.488 ALDX + 0.976 XO2H + 0.195 XO2 + 0.024 XO2N + 1.195 RO2 - 0.73 PAR	Falloff: F=0.5; n=1.13 k(0) = 8.00E-27 (T/300)^-3.5 k(inf) = 3.00E-11 (T/300)^-1	2.86E-11
143	OLE + O3 = 0.295 ALD2 + 0.555 FORM + 0.27 ALDX + 0.15 XO2H + 0.15 RO2 + 0.334 OH + 0.08 HO2 + 0.378 CO + 0.075 GLY + 0.075 MGLY + 0.09 FACD + 0.13 AACD + 0.04 H2O2 - 0.79 PAR	k = 5.50E-15 exp(-1880/T)	1.00E-17
144	OLE + NO3 = 0.5 NO2 + 0.5 NTR1 + 0.48 XO2 + 0.48 XO2H + 0.04 XO2N + RO2 + 0.5 FORM + 0.25 ALD2 + 0.375 ALDX - 1 PAR	k = 4.60E-13 exp(-1155/T)	9.54E-15
145	IOLE + O = 1.24 ALD2 + 0.66 ALDX + 0.1 XO2H + 0.1 RO2 + 0.1 CO + 0.1 PAR	k = 2.30E-11	2.30E-11
146	IOLE + OH = 1.3 ALD2 + 0.7 ALDX + XO2H + RO2	k = 1.05E-11 exp(519/T)	5.99E-11
147	IOLE + O3 = 0.732 ALD2 + 0.442 ALDX + 0.128 FORM + 0.245 CO + 0.5 OH + 0.3 XO2H + 0.3 RO2 + 0.24 GLY + 0.06 MGLY + 0.29 PAR + 0.08 AACD + 0.08 H2O2	k = 4.70E-15 exp(-1013/T)	1.57E-16

148	IOLE + NO3 = 0.5 NO2 + 0.5 NTR1 + 0.48 XO2 + 0.48 XO2H + 0.04 XO2N + RO2 + 0.5 ALD2 + 0.625 ALDX + PAR	k = 3.70E-13	3.70E-13
149	ISOP + OH = ISO2 + RO2	k = 2.70E-11 exp(390/T)	9.99E-11
150	ISOP + O = 0.75 ISPD + 0.5 FORM + 0.25 XO2 + 0.25 RO2 + 0.25 HO2 + 0.25 CXO3 + 0.25 PAR	k = 3.00E-11	3.00E-11
151	ISO2 + NO = 0.1 INTR + 0.9 NO2 + 0.673 FORM + 0.9 ISPD + 0.818 HO2 + 0.082 XO2H + 0.082 RO2	k = 2.39E-12 exp(365/T)	8.13E-12
152	ISO2 + HO2 = 0.88 ISPX + 0.12 OH + 0.12 HO2 + 0.12 FORM + 0.12 ISPD	k = 7.43E-13 exp(700/T)	7.78E-12
153	ISO2 + C2O3 = 0.598 FORM + 1 ISPD + 0.728 HO2 + 0.072 XO2H + 0.8 MEO2 + 0.2 AACD + 0.872 RO2	k = k(ref) K k(ref) = k(58) K = 1.00E+0	1.30E-11
154	ISO2 + RO2 = 0.598 FORM + 1 ISPD + 0.728 HO2 + 0.072 XO2H + 0.072 RO2	k = k(ref) K k(ref) = k(70) K = 1.00E+0	3.48E-13
155	ISO2 = HO2 + HPLD	k = 3.30E+9 exp(-8300/T)	2.64E-3
156	ISOP + O3 = 0.6 FORM + 0.65 ISPD + 0.15 ALDX + 0.2 CXO3 + 0.35 PAR + 0.266 OH + 0.2 XO2 + 0.2 RO2 + 0.066 HO2 + 0.066 CO	k = 1.03E-14 exp(-1995/T)	1.27E-17
157	ISOP + NO3 = 0.35 NO2 + 0.65 NTR2 + 0.64 XO2H + 0.33 XO2 + 0.03 XO2N + RO2 + 0.35 FORM + 0.35 ISPD	k = 3.03E-12 exp(-448/T)	6.74E-13
158	ISPD + OH = 0.022 XO2N + 0.521 XO2 + 0.115 MGLY + 0.115 MEO2 + 0.269 GLYD + 0.269 C2O3 + 0.457 OPO3 + 0.117 PAR + 0.137 ACET + 0.137 CO + 0.137 HO2 + 0.658 RO2	k = 5.58E-12 exp(511/T)	3.10E-11
159	ISPD + O3 = 0.04 ALD2 + 0.231 FORM + 0.531 MGLY + 0.17 GLY + 0.17 ACET + 0.543 CO + 0.461 OH + 0.15 FACD + 0.398 HO2 + 0.143 C2O3	k = 3.88E-15 exp(-1770/T)	1.02E-17
160	ISPD + NO3 = 0.717 HNO3 + 0.142 NTR2 + 0.142 NO2 + 0.142 XO2 + 0.142 XO2H + 0.113 GLYD + 0.113 MGLY + 0.717 PAR + 0.717 CXO3 + 0.284 RO2	k = 4.10E-12 exp(-1860/T)	7.98E-15
161	ISPD = 0.76 HO2 + 0.34 XO2H + 0.16 XO2 + 0.34 MEO2 + 0.208 C2O3 + 0.26 FORM + 0.24 OLE + 0.24 PAR + 0.17 ACET + 0.128 GLYD + 0.84 RO2	Photolysis	1.60E-5
162	ISPX + OH = 0.904 EPOX + 0.933 OH + 0.067 ISO2 + 0.067 RO2 + 0.029 IOLE + 0.029 ALDX	k = 2.23E-11 exp(372/T)	7.77E-11
163	HPLD = OH + ISPD	Photolysis	4.41E-4
164	HPLD + NO3 = HNO3 + ISPD	k = 6.00E-12 exp(-1860/T)	1.17E-14
165	EPOX + OH = EPX2 + RO2	k = 5.78E-11 exp(-400/T)	1.51E-11
166	EPX2 + HO2 = 0.275 GLYD + 0.275 GLY + 0.275 MGLY + 1.125 OH + 0.825 HO2 + 0.375 FORM + 0.074 FACD + 0.251 CO + 2.175 PAR	k = 7.43E-13 exp(700/T)	7.78E-12
167	EPX2 + NO = 0.275 GLYD + 0.275 GLY + 0.275 MGLY + 0.125 OH + 0.825 HO2 + 0.375	k = 2.39E-12 exp(365/T)	8.13E-12

	FORM + NO2 + 0.251 CO + 2.175 PAR		
168	EPX2 + C2O3 = 0.22 GLYD + 0.22 GLY + 0.22 MGLY + 0.1 OH + 0.66 HO2 + 0.3 FORM + 0.2 CO + 1.74 PAR + 0.8 MEO2 + 0.2 AACD + 0.8 RO2	k = k(ref) K k(ref) = k(58) K = 1.00E+0	1.30E-11
169	EPX2 + RO2 = 0.275 GLYD + 0.275 GLY + 0.275 MGLY + 0.125 OH + 0.825 HO2 + 0.375 FORM + 0.251 CO + 2.175 PAR + RO2	k = k(ref) K k(ref) = k(70) K = 1.00E+0	3.48E-13
170	INTR + OH = 0.63 XO2 + 0.37 XO2H + RO2 + 0.444 NO2 + 0.185 NO3 + 0.104 INTR + 0.592 FORM + 0.331 GLYD + 0.185 FACD + 2.7 PAR + 0.098 OLE + 0.078 ALDX + 0.266 NTR2	k = 3.10E-11	3.10E-11
171	TERP + O = 0.15 ALDX + 5.12 PAR	k = 3.60E-11	3.60E-11
172	TERP + OH = 0.75 XO2H + 0.5 XO2 + 0.25 XO2N + 1.5 RO2 + 0.28 FORM + 1.66 PAR + 0.47 ALDX	k = 1.50E-11 exp(449/T)	6.77E-11
173	TERP + O3 = 0.57 OH + 0.07 XO2H + 0.69 XO2 + 0.18 XO2N + 0.94 RO2 + 0.24 FORM + 0.001 CO + 7 PAR + 0.21 ALDX + 0.39 CXO3	k = 1.20E-15 exp(-821/T)	7.63E-17
174	TERP + NO3 = 0.47 NO2 + 0.28 XO2H + 0.75 XO2 + 0.25 XO2N + 1.28 RO2 + 0.47 ALDX + 0.53 NTR2	k = 3.70E-12 exp(175/T)	6.66E-12
175	BENZ + OH = 0.53 CRES + 0.352 BZO2 + 0.352 RO2 + 0.118 OPEN + 0.118 OH + 0.53 HO2	k = 2.30E-12 exp(-190/T)	1.22E-12
176	BZO2 + NO = 0.918 NO2 + 0.082 NTR2 + 0.918 GLY + 0.918 OPEN + 0.918 HO2	k = 2.70E-12 exp(360/T)	9.04E-12
177	BZO2 + C2O3 = GLY + OPEN + HO2 + MEO2 + RO2	k = k(ref) K k(ref) = k(58) K = 1.00E+0	1.30E-11
178	BZO2 + HO2 =	k = 1.90E-13 exp(1300/T)	1.49E-11
179	BZO2 + RO2 = GLY + OPEN + HO2 + RO2	k = k(ref) K k(ref) = k(70) K = 1.00E+0	3.48E-13
180	TOL + OH = 0.18 CRES + 0.65 TO2 + 0.72 RO2 + 0.1 OPEN + 0.1 OH + 0.07 XO2H + 0.18 HO2	k = 1.80E-12 exp(340/T)	5.63E-12
181	TO2 + NO = 0.86 NO2 + 0.14 NTR2 + 0.417 GLY + 0.443 MGLY + 0.66 OPEN + 0.2 XOPN + 0.86 HO2	k = 2.70E-12 exp(360/T)	9.04E-12
182	TO2 + C2O3 = 0.48 GLY + 0.52 MGLY + 0.77 OPEN + 0.23 XOPN + HO2 + MEO2 + RO2	k = k(ref) K k(ref) = k(58) K = 1.00E+0	1.30E-11
183	TO2 + HO2 =	k = 1.90E-13 exp(1300/T)	1.49E-11
184	TO2 + RO2 = 0.48 GLY + 0.52 MGLY + 0.77 OPEN + 0.23 XOPN + HO2 + RO2	k = k(ref) K k(ref) = k(70) K = 1.00E+0	3.48E-13
185	XYL + OH = 0.155 CRES + 0.544 XLO2 + 0.602 RO2 + 0.244 XOPN + 0.244 OH + 0.058 XO2H + 0.155 HO2	k = 1.85E-11	1.85E-11
186	XLO2 + NO = 0.86 NO2 + 0.14 NTR2 + 0.221 GLY + 0.675 MGLY + 0.3 OPEN + 0.56 XOPN + 0.86 HO2	k = 2.70E-12 exp(360/T)	9.04E-12

187	XLO2 + HO2 =	k = 1.90E-13 exp(1300/T)	1.49E-11
188	XLO2 + C2O3 = 0.26 GLY + 0.77 MGLY + 0.35 OPEN + 0.65 XOPN + HO2 + MEO2 + RO2	k = k(ref) K k(ref) = k(58) K = 1.00E+0	1.30E-11
189	XLO2 + RO2 = 0.26 GLY + 0.77 MGLY + 0.35 OPEN + 0.65 XOPN + HO2 + RO2	k = k(ref) K k(ref) = k(70) K = 1.00E+0	3.48E-13
190	CRES + OH = 0.025 GLY + 0.025 OPEN + HO2 + 0.2 CRO + 0.732 CAT1 + 0.02 XO2N + 0.02 RO2	k = 1.70E-12 exp(950/T)	4.12E-11
191	CRES + NO3 = 0.3 CRO + HNO3 + 0.48 XO2 + 0.12 XO2H + 0.24 GLY + 0.24 MGLY + 0.48 OPO3 + 0.1 XO2N + 0.7 RO2	k = 1.40E-11	1.40E-11
192	CRO + NO2 = CRON	k = 2.10E-12	2.10E-12
193	CRO + HO2 = CRES	k = 5.50E-12	5.50E-12
194	CRON + OH = NTR2 + 0.5 CRO	k = 1.53E-12	1.53E-12
195	CRON + NO3 = NTR2 + 0.5 CRO + HNO3	k = 3.80E-12	3.80E-12
196	CRON = HONO + HO2 + FORM + OPEN	Photolysis	9.45E-5
197	XOPN = 0.4 GLY + XO2H + 0.7 HO2 + 0.7 CO + 0.3 C2O3	Photolysis	5.04E-4
198	XOPN + OH = MGLY + 0.4 GLY + 2 XO2H + 2 RO2	k = 9.00E-11	9.00E-11
199	XOPN + O3 = 1.2 MGLY + 0.5 OH + 0.6 C2O3 + 0.1 ALD2 + 0.5 CO + 0.3 XO2H + 0.3 RO2	k = 1.08E-16 exp(-500/T)	2.02E-17
200	XOPN + NO3 = 0.5 NO2 + 0.5 NTR2 + 0.45 XO2H + 0.45 XO2 + 0.1 XO2N + RO2 + 0.25 OPEN + 0.25 MGLY	k = 3.00E-12	3.00E-12
201	OPEN = OPO3 + HO2 + CO	Photolysis	5.04E-4
202	OPEN + OH = 0.6 OPO3 + 0.4 XO2H + 0.4 RO2 + 0.4 GLY	k = 4.40E-11	4.40E-11
203	OPEN + O3 = 1.4 GLY + 0.24 MGLY + 0.5 OH + 0.12 C2O3 + 0.08 FORM + 0.02 ALD2 + 1.98 CO + 0.56 HO2	k = 5.40E-17 exp(-500/T)	1.01E-17
204	OPEN + NO3 = OPO3 + HNO3	k = 3.80E-12	3.80E-12
205	CAT1 + OH = 0.14 FORM + 0.2 HO2 + 0.5 CRO	k = 5.00E-11	5.00E-11
206	CAT1 + NO3 = CRO + HNO3	k = 1.70E-10	1.70E-10
207	OPO3 + NO = NO2 + 0.5 GLY + 0.5 CO + 0.8 HO2 + 0.2 CXO3	k = 1.00E-11	1.00E-11
208	OPO3 + NO2 = OPAN	k = k(ref) K k(ref) = k(54) K = 1.00E+0	9.40E-12
209	OPAN = OPO3 + NO2	k = k(ref) K k(ref) = k(55) K = 1.00E+0	2.98E-4
210	OPO3 + HO2 = 0.41 PACD + 0.15 AACD + 0.15 O3 + 0.44 ALDX + 0.44 XO2H + 0.44 RO2 + 0.44 OH	k = k(ref) K k(ref) = k(57) K = 1.00E+0	1.39E-11
211	OPO3 + C2O3 = MEO2 + XO2 + ALDX + 2 RO2	k = k(ref) K k(ref) = k(59) K = 1.00E+0	1.55E-11

212	OPO3 + RO2 = 0.8 XO2H + 0.8 ALDX + 1.8 RO2 + 0.2 AACD	k = k(ref) K k(ref) = k(58) K = 1.00E+0	1.30E-11
213	OPAN + OH = 0.5 NO2 + 0.5 GLY + CO + 0.5 NTR2	k = 3.60E-11	3.60E-11
214	PANX + OH = ALD2 + NO2	k = 3.00E-12	3.00E-12
215	NTR2 = HNO3	k = 2.30E-5	2.30E-5
216	ECH4 + OH = MEO2 + RO2	k = 1.85E-12 exp(-1690/T)	6.37E-15
217	XPRP = XO2N + RO2	Falloff: F=0.41; n=1 k(0) = 2.37E-21 k(inf) = 4.30E-1 (T/298)^-8	3.09E-2
218	XPRP = 0.732 ACET + 0.268 ALDX + 0.268 PAR + XO2H + RO2	k = 1.00E+0	1.00E+0
219	XPAR = XO2N + RO2	Falloff: F=0.41; n=1 k(0) = 4.81E-20 k(inf) = 4.30E-1 (T/298)^-8	1.49E-1
220	XPAR = 0.126 ALDX + 0.874 ROR + 0.126 XO2H + 0.874 XO2 + RO2 -0.126 PAR	k = 1.00E+0	1.00E+0